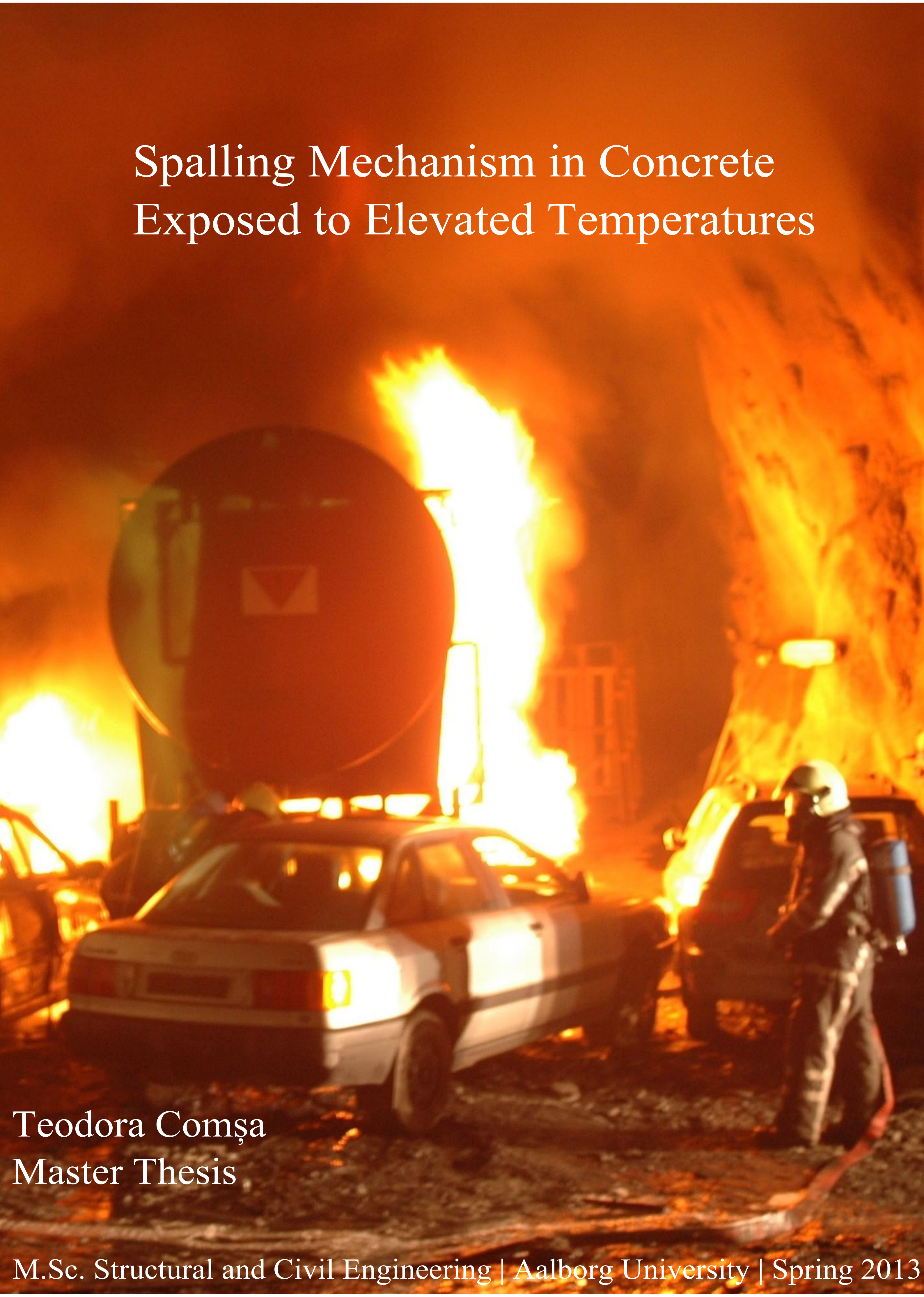

Spalling Mechanism in Concrete Exposed to Elevated Temperatures

Teodora Comșa
Master Thesis

M.Sc. Structural and Civil Engineering | Aalborg University | Spring 2013

AALBORG UNIVERSITET

Institut for Byggeri & Anlæg
Sohngårdsholmsvej 57
9000 Aalborg
Telefon: +45 99 40 85 30
http://www.bsn.aau.dk

Title:
Spalling mechanism in concrete exposed to elevated temperatures

Project period:
Master Thesis, spring 2013

Project group:
B207

Student:
Teodora Comsa

Supervisors:
Lars Damkilde
Poul Henning Kirkegaard

Circulation numbers: 2

Page numbers: 79

Completed:
Thursday the 15th of August 2013

Synopsis:

This report presents the description of the spalling mechanism of a concrete member exposed to fire. The theory behind the phenomenon is explained along with failure due to different types of loading and also the fire behavior of high performance concrete (HPC), self-compacting concrete (SCC) and high strength concrete (HSC) based on experimental results. Concrete properties and comportment in fire are presented in order to further on use them for modeling a simplified physical model. The physical model is divided into a thermo-hygral (taking into account the mass and heat transport process) and a mechanical model (accounting for developing of thermal and shrinkage strains). Following these ideas, a mathematical model and later on a 1-D numerical model are provided. The results validate some of the theoretical assumptions made in the beginning. In the end, conclusions and recommendations for further development are made based on the whole report.

Preface and reading guide

This report is the product of the project work of group B207, which consists of a single student member from the 4st semester of the master program in Structural and Civil Engineering at Aalborg University. The title of the project is *Spalling mechanism in concrete exposed to elevated temperatures.* The project has been conducted with the guidance and help from supervisors Lars Damkilde and Poul Henning Kirkegaard.

The project is divided into nine main parts, that also represents the chapters of the report. Each chapter contains a number of sections and subsections that presents the theory, assumptions and results. During the processing of the main report references will appear, and these will be collected in a bibliography in the back of the main report. Sources are presented when it is relevant using the *Harvard method*, where a source in the text is referred to as [Surname, Year]. If there are more than one author, these are indicated by 'et al.'. If the same author appears several times, the surnames will also be alphabetically ordered. A reference leads to the bibliography, where books are listed with author, title, edition and possible publishers, while websites are indicated by author, title and the date where it is used.

Figures and tables are numbered according to chapter in which they are present. Therefore, the first figure in chapter 3 number 3.1, the second number is 3.2, etc. Explanatory text for figures and tables can be found under the given figures and tables, like the source is set for figures or tables that are not produced by the project group itself. Formulas, equations and expressions are indicated by number in parentheses, where the numbering is similar to figures and tables.

Teodora Comsa

Contents

CHAPTER 1

Outline of the thesis

The main objective of this thesis is to provide a one dimensional numerical model for the phenomenon of concrete spalling. For this to be achieved knowledge about concrete properties and behavior at elevated temperatures is needed. Also previous work on the subject needs to be investigated.

The model consists in applying mathematical equations for physical phenomena and transforming them into finite element formulations.

A second objective is to study the influencing factors of spalling, such as the moisture content, gas pressure and heating rate and state some conclusion about their contribution.

A third and last scope is the study of strains and stresses developed during the process and appreciate the damage they can cause for the member.

In order to get an overview of the content in the project report an illustration of the steps followed can be seen in figure 1.1. In the introduction general concepts about fire safety design and construction materials behavior in fire are provided as well as difficulties related to concrete damage evaluation. A theoretical description of concrete spalling followed by different loads types inducing failure and comportment of different types of concrete is given. Thermal, hygral and mechanical properties of concrete are exposed. Based on this, a physical model is provided. Starting from the division of the physical model, a mathematical and numerical model is given. Some of the results are compared with experimental outcomes. All the results are commented and conclusions are exposed.

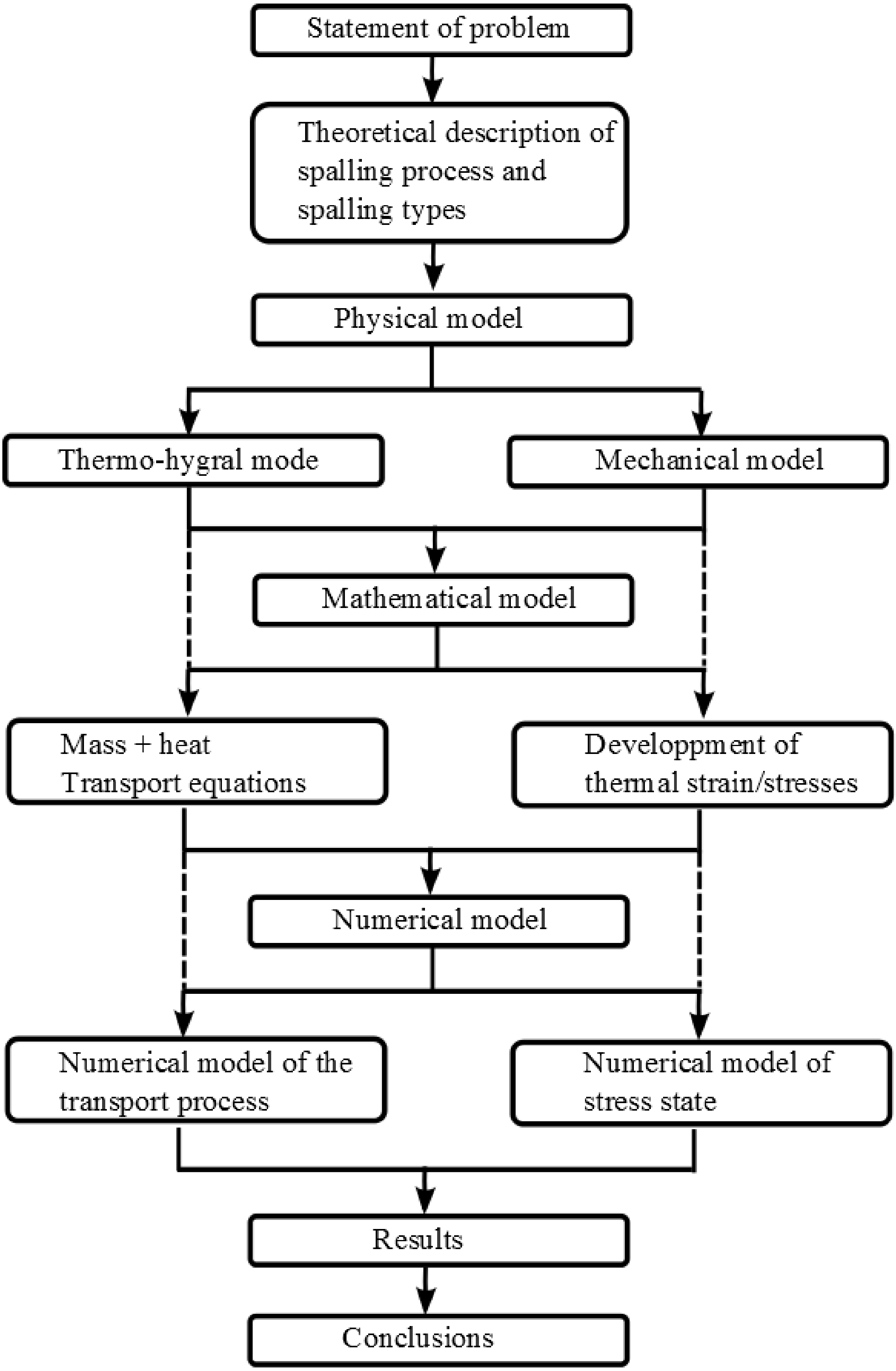

Figure 1.1. Project content

Chapter 2

Introduction

An introduction to the fire safety design of buildings and short descriptions of steel and timber behavior at elevated temperatures is given. Brief notions about the fire design concepts are illustrates for both steel and timber. Concrete development in time along with types of concrete is exposed. Conceptual design methods for concrete should involve spalling, because of its high risks of occurrence especially in "new" types of concrete. In the end, a conclusion is pointed out about damage assessment of different building materials at elevated temperatures.

2.1 Fire design

When designing a building or an infrastructure there are several environmental hazards that should be taken into account. Maybe one of the most severe ones is fire.

Fire safety design refers to two strategies, depending on the evolution of fire: in the early stages of a fire the aim is to prevent fire spreading outside the compartment to other parts of the building and in the latter structural collapse. The first one can be achieved by sprinklers, fans or other devices against smoke or suitable materials and interior linings that retard flame spread. If fire keeps growing despite the previous presented measures, the structure needs to have sufficient fire resistance to remain structurally stable for a period of time. Therefore, an important and critical parameter involved in these strategies is *time*.

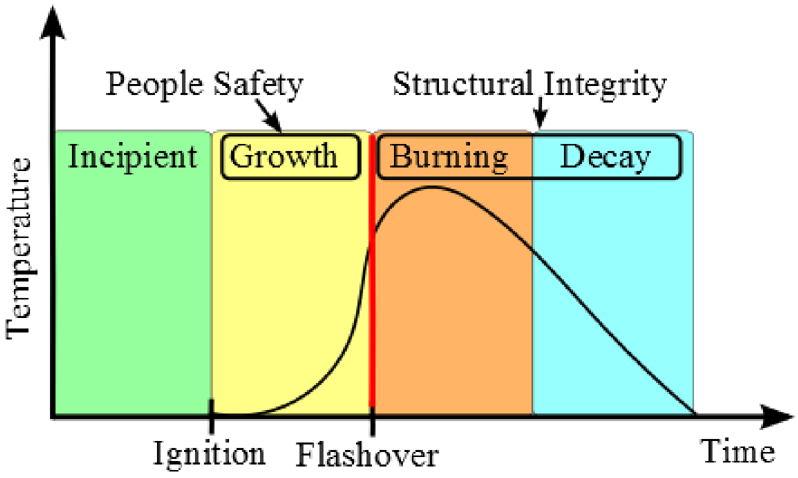

Figure 2.1. Fire evolution, inspired by [Buchanan, 2001]

Figure 2.1 presents the fire process development inside a room assuming there are no suppression devices or fire fighters to stop the fire evolution. Of course, not all room fires follow this trend, depending on the ventilation factors, material linings, etc. The stages of interest are the growth period in terms of people safety and the burning and decay period, from a structural point of view (in this stage there are no survivals, the temperatures can reach values of 1200°C). The flashover cannot be defined as a precise term but more like a transitions phase between the growth (pre-flashover) and the burning period, known also as a fully developed stage or post-flashover. In this thesis, only the burning phase is taken into account.

Therefore, the structural engineers task is to take enough measures when designing so that there is sufficient time to ensure safe escape for people and structural integrity and stability of the building itself. Time is closely related to type of material used for design: steel, timber or concrete.

2.2 Steel behavior and design at elevated temperatures

The behavior of steel members depends very much if the member is protected or unprotected. Unprotected members exhibit large deformations during fires while well-protected ones can have small or even no damage. Even though steel members can suffer high damage during a fire, they have also the property of recovering after heating. If heated up to temperatures of 600°C common grades of structural steel do not undergo significant strength loss when cooled and higher temperatures can reduce the strength up to about 10%, [Buchanan, 2001].

Fire design for steel is relatively easy due to similarities with steel design at ambient temperatures, the only changes that need to be taken into account are regarding reduction of yield strength and modulus of elasticity, both decreasing as temperature increases (practically speaking, the two mechanical properties are multiplied with a correction factor that considers the temperature effect). Aspects related to the geometry of the section and deformation capacity, classified in the Eurocode as steel classes regarding susceptibility to local buckling are also taken into account.

Figure 2.2 shows a steel beam to column connection after fire exposure. Local buckling of the beams can be observed while the column does not undergo visible deformation. According to [Buchanan, 2001], in most cases no further assessment is needed for remaining straight members after fire. Anyway, hardness test or tensile tests can be carried out to determine exactly the strength reduction. This situation is a good example of geometry dependency and residual capacity after fire.

Figure 2.2. Steel connection after fire exposure [Lamont, 2006]

2.3 Timber behavior and design at elevated temperature

Figure 2.3 illustrates what happens with a timber member when exposed to fire. As seen, the surface ignites and burns rapidly. The burned material becomes a char layer which protects the wood below. The char layer contains a char base followed by a pyrolysis zone and a pyrolysis zone base. After this normal wood can be found. When heated above 100°C, the moisture in the layer bellow the char layer evaporates. Some part of the evaporated moisture runs out to the burning face and the other part travels inside the wood, increasing the moisture content in the heated wood. Briefly, wood properties are affected by steam at 100°C, pyrolysing begins around 200°C and turns into char at 300°C, interest in design for timber structures involving room temperature to 300°C, [Buchanan, 2001].

Fire design of timber structures involves some complications compared to common materials like steel or concrete because of its thermal properties that vary considerably depending on species, for example density, and sometimes are not even well defined (thermal conductivity) etc. Other aspects concern mechanical properties that are also different depending on the direction (parallel and perpendicular to the grain), strength and ductility, failure stresses (depending on specimen size), several failure modes, etc.

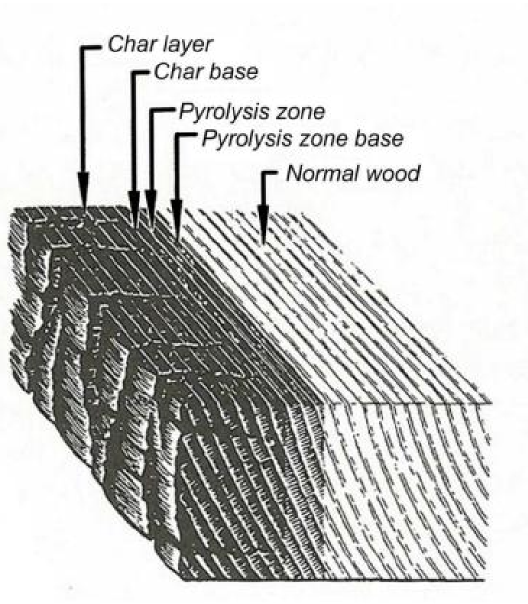

Figure 2.3. Developed layers in timber beam exposed to fire,[Buchanan, 2001]

The design concepts are simplified and therefore take into account only the "cold" wood, the original section being reduced to a residual cross section due to charring, as seen in figure 2.4. The depth of charring can be calculated using the rate of charring, β (mm/min). There are different values for β, according to different codes and experiment results. An approximate value can considered around 1mm/min.

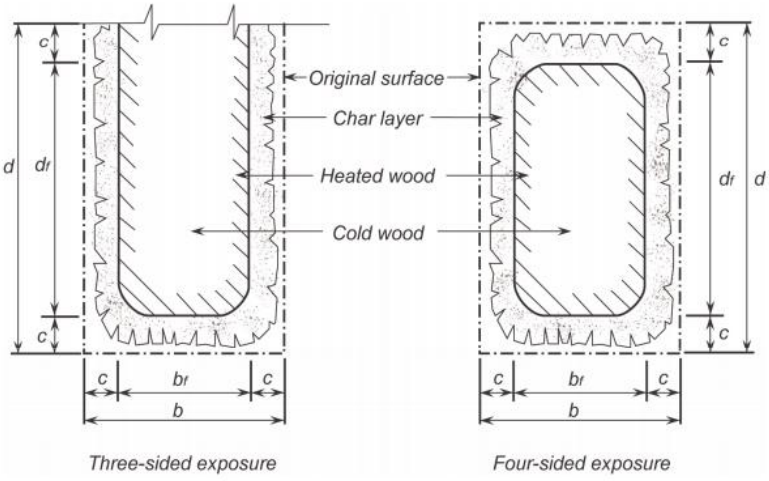

Figure 2.4. Design concepts for timber members [Buchanan, 2001]

Within the design methods, the most used and realistic ones are *The effective cross section method* and *The reduced properties method* presented in Eurocode 5. The first one considers a smaller cross section than the residual one, assuming a layer with zero strength wood below the char line and material properties identical with ones at ambient temperature in the inner part. The second one uses the geometry of the first method, but reduced material properties over the entire residual cross section.

Another thing that requires special attention are the timber connections. Depending on their nature, metal fasteners or adhesives, they have also very different fire performance. The principal idea is that the connections should have at least the same fire resistance as the main member. Regarding this field, still there is few information and most mathematical models rely on empirical approaches.

2.4 Concrete design guidance and spalling considerations

Concrete is one of the most used building materials in the world. It has been used since Roman times and has been through changes ever since. From the moment that reinforced concrete developed, the construction department encountered a fast growth. Combination of concrete and steel, with different properties leads to a material with both compression and tension strength, and larger fields of application. Later, use of fibers instead of reinforcement started to be the point of interest for many researchers. Other changes within the composition of concrete like reduction of water content, use of new types of additives or superplasticizers that can replace partially or totally the Portland cement, optimization of grain size distribution, etc. made it possible to obtain new concretes and mortars with improvements of their properties such as strength, workability, ductility, compactness, rheology, electrical conductivity and so on.

Compared to steel, where the material is homogeneous and timber, where simplifications make the design easy, when dealing with concrete fire design, there are many parameters involved and simplifications could lead to wrong prediction of the concrete member performances. Fire design for normal concrete is similar to some extent to timber design. Here the *The 500° C isotherm method* and *The zone method* are implied. The first one considers a reduced section of the initial member, where the temperature is below 500°C and then the bearing capacity is evaluated following usual calculation procedures. The reduction in strength of each reinforcement rebar is worked out. The second method consists in dividing the section in parallel zones with the isothermal lines. The reduction zone is identified based on the evaluated damage of each zone taking into account the average temperatures of the different zones. After knowing the reduced zone, usual procedures can be applied.

But when it comes to design of "new concretes", more unknowns develop which make the design more difficult. Between the "new" concretes, high performance concrete, high strength concrete, ultra high strength concrete and self-compacting concrete are significant examples. Although at ambient temperature these concretes behave better than the normal concrete from the mechanical point of view, when exposed to fire conditions, spalling has a higher probability of occurrence for them. Phenomena like progressive spalling characterised by a gradual fall out of small pieces of concrete from the element surface or impulsive failure with great release of energy and fall out of large pieces of material, in the case of explosive spalling, can seriously jeopardize the load- bearing capacity of the structure, and, in the worst scenario can lead to complete failure of the element. An example of spalling can be seen in figure 2.5.

Figure 2.5. Seriously damaged circular columns (Explosive spalling) [Yaquba et al., 2011]

Spalling has serious structural and economic consequences, as for example fire in tunnels: the*Mont Blanc* or *Channel* tunnel fires that needed large costs of repairing and retroffiting after the conflagration, but also large indirect economic damage due to long non- operational times, [Beard and Carvel, 2005]. For this reason spalling should be taken into account when designing for fire resistance. Being a function of several different factors such as temperature, moisture content, vapor pressure, concrete type, cement paste, etc., it is difficult to fully understand the mechanism behind spalling and to quantify the risk of it to occur.

According to [Buchanan, 2001], the best economical method to prevent spalling is the addition of fine polypropylene fibers to the concrete mix within a range of 0.15% to 0.3%. During fire exposure, the polypropylene fibers melt and therefore increase the porosity of the element by creating cavities through which water vapor can escape. In this way the likelihood of spalling is decreased.

Therefore, with these new materials, also a new approach of building design is required. Technical solutions should focus on improving the structural design within parameters such as type of reinforcement, external protection, element dimensions but also factors as the microstructure of the material, aggregate mix, cement paste, etc. Concerning people safety, until further development, usage of these concretes should be limited to lower areas of fire risk, for example foundations, [P.Kalifa et al., 2000].

2.5 General remarks

Summing up all the data presented above it can be seen that fire design involves peoples safety as well as structural integrity and stability. Fire design depends on the type of chosen material as different building materials have different behavior at elevated temperatures. The general idea concerning structural design present in the codes is based on the concepts used for ambient temperatures, but including also parameters for fire effect.

For steel, in most of the cases the damage after fire can be assessed visually, members that are still straight do no need to be replaced and buckling in steel members can easily be identified. Also, steel has the advantageous property of recovering after fires.

When dealing with timber, the damage assessment can be measured and observed with the naked eye, the region from the surface until normal wood is burned, phenomena noticeable by the difference in colors (black for the char layer and brown as usual wood color for the normal wood layer). The damaged layer is removed and then the residual cross section can be used further on in some cases.

When it comes to concrete, because of its heterogeneous character, things are not that simple anymore. The assessment cannot be performed only visually. It some cases, if the member was damaged severely, as for example in figure 2.5, it can be concluded that the member cannot longer be in use. But in some other cases, when the damage is not that obvious, as for local spalling, cracking or damage that goes beneath the surface element, further investigation (nondestructive and/or destructive tests) needs to be carried out in order to decide if the element can still be used and the level of repair it demands. For an easier evaluation of the damage, the design procedure should involve parameters that include spalling occurrence. Although a global solution cannot be adopted at this stage, due to the before stated arguments, approximated numerical models as a result of good understanding of the process can be implemented. The models should be elementary instruments defined in a way able to prevent and predict behavior of concrete structures exposed to high temperatures.

For this, in the very beginning the physical process of spalling should be examined in order to further have a better understanding of developing a simple physical model or more complicated models, like the mathematical and numerical ones.

CHAPTER 3

Description of Spalling and Types of Loading Inducing Failure

Spalling is defined and then analytical and numerical results based on the described mechanism are exposed. Different types of spalling and factors inducing it are presented: pore pressure spalling, thermal stress spalling and thermal cracking spalling. Spalling test results from high performance concrete, high strength concrete and self compacting concrete will be exposed and an overview about the outcome will be analyzed.

3.1 Definition and types of spalling

From a simple perspective, spalling might be defined as a separation of concrete from the surface of a concrete element when heated,[Bažant and Kaplan, 1996], as seen in figure 3.1.

Figure 3.1. Example of fire spalling of concrete:the Mont Blanc tunnel [der Heijden, 2006]

This separation can happen in different ways, as classified by the Institution of Structural Engineers, 1975:

1. *General or destructive spalling:* "This is a violent form of spalling which occurs at an early stage of heating and may result in extensive damage or complete destruction of the concrete element."

2. *Local spalling:* "This consists of sometimes violent surface spalling, aggregate splitting or corner separation. Aggregate spalling is caused by aggregate failure close to the surface and involves small pieces flying off from the surface. This type of spalling does not adversely affect the structural performance, causing only superficial damage."
3. *Sloughing off:* "This is a progressive form of breakdown which involves partial separation of material from the concrete element. Corner spalling occurs later, often in the decay stages of the fire. It is characterized by larger corner pieces falling off the concrete due to tensile cracks developing at corners and edges. Due to the late onset of this type of spalling the concrete affected is already considerably weakened from fire exposure and any exposed reinforcement is subjected to much lower temperatures. Thus corner spalling is not thought to have a significant impact on structural fire performance."

Due to the fact that explosive spalling poses the greater threat to structural stability this form will be investigated in more detail. In current design codes like [EC2-EN1992-1-2, 2005], there is not much information about spalling. It is stated that no checks for spalling are necessary if the moisture content of the member is less than 3% or the member is designed for internal exposure and that the tabulated data is used to prescribe generic fire ratings for concrete elements (except for axis distances $>$ 70 mm). For concrete grades $80/95 < C \leqslant 90/105$ spalling can occur in any situation for concrete exposed directly to the fire and four methods are recommended to be used, regarding reinforcement mesh, type of concrete, protective layers and inclusion in the concrete mix of more than $2kg/m^3$ of monofilament propylene fibers.

3.2 Spalling mechanism

The spalling mechanism is illustrated in figure 3.2. As the heat flows into the porous medium, the water inside the element will evaporate at temperatures above 100°C and a part of it will flow out of the concrete member, passing the "dry" zone, effect that is also visible by the steams coming out of the member while the other part will flow inside the porous medium, depending on the permeability of the material (high permeability will allow more vapor migration out of the medium).

The water vapors flowing inside the member will condensate again into water when encountering regions with temperatures lower than 100°C and they will be reabsorbed into the pores of the member. This reabsorbed water together with the present evaporable water will form a saturated layer, called "moisture clog" that prevents any gas flow from going further into the medium. If the permeability of the material is not sufficient enough to avoid a continuous pressure build-up because of vaporization then spalling is possible to occur, figure 3.2(d).

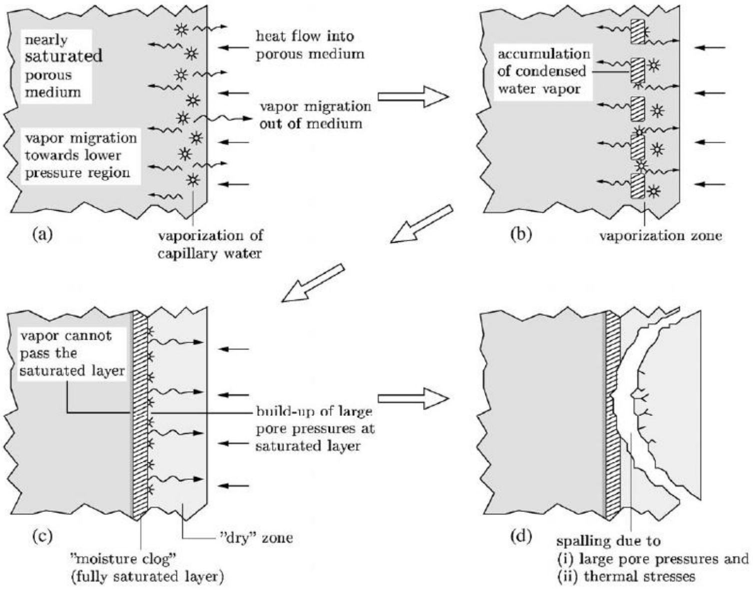

Figure 3.2. Numerical modeling of spalling [M.Zeiml et al., 2005]

3.2.1 Analytical and numerical results based on the spalling mechanism

Based on the above description of the physical model of spalling, there are a lot of analytical, experimental and numerical approaches. Among the existing examples, two will be briefly illustrated in the following.

An analytical model was made by [van der Heijin and van Bijnen, 2007] and exposed in *"Moisture transport in heated concrete, as studied by NMR and its consequence for fire spalling"* article.

The model tries to predict the position of the drying front by calculating analytically the temperature and vapor flux within the element. The outcome is compared with experimental results.

Figure 3.3 shows the calculation results, the solid line, the experimental ones, the pointed line and the reference position of the 100°C is showed with dashed line. A good correlation between calculations and experiment can be seen.

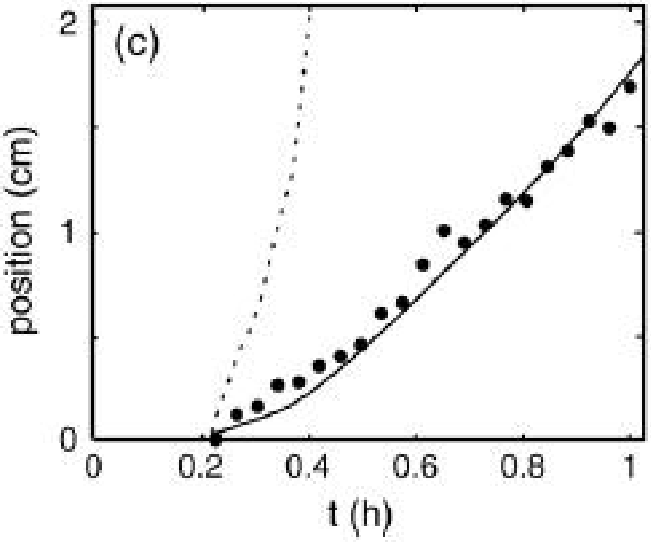

Figure 3.3. Analytical results of the drying front, [van der Heijin and van Bijnen, 2007]

[D.Gawin et al., 2005] in their article *"Towards prediction of the thermal spalling risk through a multi-phase porous media model of concrete"* present a more complicated model taking into account the multiphase nature of concrete (medium which pores contains more than one liquid), moisture behavior, load induced thermal strain, deformation of heated concrete, cracking, thermo-chemical deterioration of concrete and change of material properties. Their model was computed using *The finite element method.*

The results for the "moisture clog" can be seen in figure 3.4. The relative humidity is 0 in the "dry" zone and then moving forward into the element it increases and reaches its maximum where the saturated layer is formed, its position varying in time.

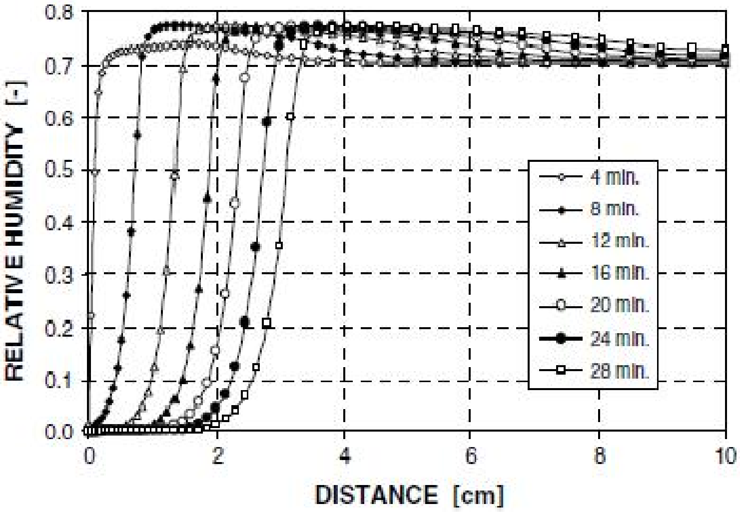

Figure 3.4. Numerical results for the "moisture clog", [D.Gawin et al., 2005]

3.2.2 Failure mechanism due to different types of loading

The mechanism of explosive spalling was explained before. The reasons that contribute to this can be divided in three types of loading categories: spalling due to pore pressure, spalling due to thermal stress and spalling due to thermal cracking, [Fu and Li, 2010].

3.2.2.1 Pore pressure spalling

In this case, a build-up of high pore pressures and severe gradients results as a consequence of migration of air, vapor and liquid water in the porous network, as seen in picture 3.5. While temperature increases, some part of the water is evaporated through the surface, and the other part is transferred into the interior of the element where vapor condenses again if the temperature is below 100°C. As a result, a quasi-saturated layer is formed.

Now the material can be divided into three zones: (1) dry and dehydrated zone, (2) drying and dehydrating zone, (3) quasi-saturated layer that acts as an impermeable wall for vapor release, and (4) unchanged zone far away from its heated surface, where the material satisfies same conditions as before fire. The pressure peak is situated in the saturated layer (moisture clog). The formation of the moisture clog depends on the permeability of the material, the lower the permeability the faster the moisture clog develops and the higher the pressure is and its pressure gradient, [Fu and Li, 2010].

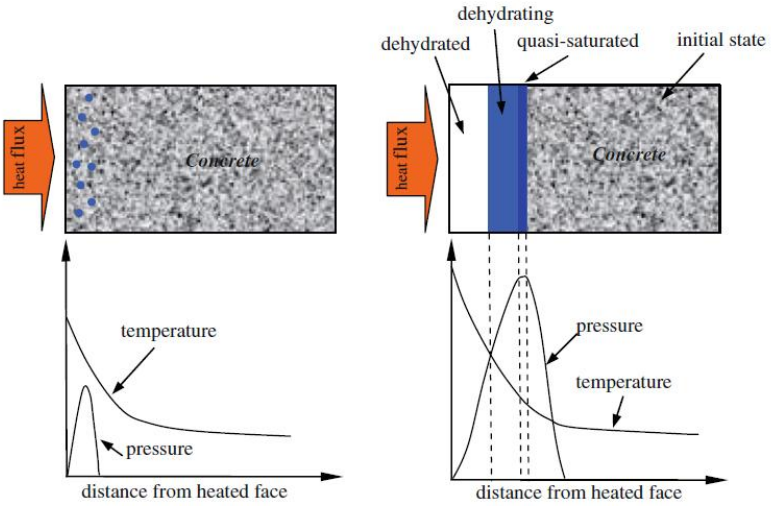

Figure 3.5. The process for the build-up of pressure [M.Zeiml et al., 2005]

3.2.2.2 Thermal stress spalling

This type of spalling is due to rapid heating that generates excessive thermal stresses, and this is a proof that other factors than pore pressures may contribute to explosive spalling. Severe thermal gradients that induce thermal shock will generate high compressive stresses close to the heated surface due to restrained thermal expansion and tensile stresses in the cooler interior regions, (see figure 3.6). With temperature increase the aggregates dilate until they degraded chemically generating tension and the cement paste shrinks as soon as water escapes generating compression of the material, this leading to strain incompatibilities, [Fu and Li, 2010].

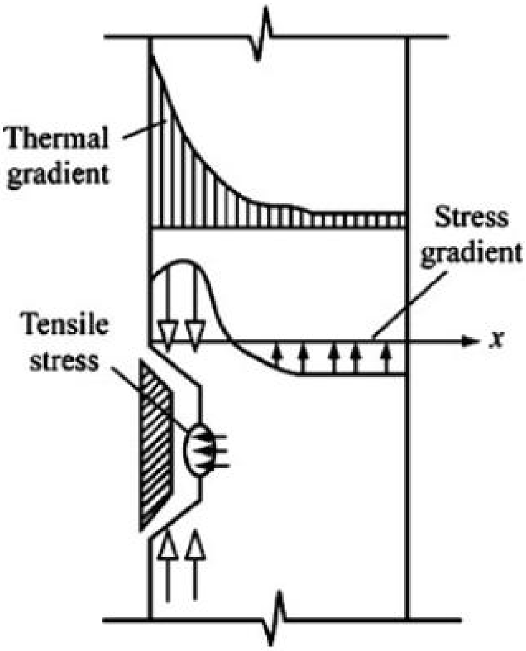

Figure 3.6. Mechanism of thermal stress spalling [Fu and Li, 2010]

3.2.3 Thermal cracking spalling

This case takes into account the heterogeneity of the concrete. Internal cracks in concrete within high heating rate can be influenced by factors as, without taking into account any external loading: release of absorbed and chemically bound water, thermal mismatch stress between aggregates and cement paste, temperature gradient, decomposition of hydration, [Fu and Li, 2010].
Thermal cracks can be divided in three types:(a) shrinkage cracks induced by the decomposition of hydration; (b) TMS cracks (radial, tangential and aggregate cracks) induced by the thermal mismatch between the aggregate and the hardened cement paste, and (c) internal and external cracks induced by temperature gradients, [Fu and Li, 2010].

As seen from the different spalling mechanisms presented above, it can be stated that spalling is related to generation of pore pressures and development of cracks, which in turn are influenced by the heating rate and the heterogeneous composition of the concrete.

3.3 Spalling in different types of concretes

3.3.0.1 High performance concrete (HPC)

According to [P.Kalifa et al., 2000], the high compactness of HPC is the main parameter responsible for spalling at high temperatures. When comparing experimentally a normal concrete (M30,w/c=0.5) with a HPC concrete(M100, w/c=0.32), both with calcareous aggregates, it could be noticed that they have globally a similar thermal behavior, related with their similar thermal properties (thermal conductivity and specific heat) . The difference comes when measuring the pore pressure, up to 38 bars in the HPC and 18 bars in the normal concrete; as well HPC underwent higher pressure gradients than normal concrete.

It can be stated that as a consequence of lower permeability (to vapor and liquid water), there is a large difference in the thermodynamic conditions reached in the porous network, which results in much higher pore pressures.

3.3.0.2 High strength concrete (HSC)

Tests ran by [Bastami et al., 2011] on HSC were done on 16 samples, 12 with silica fume mixtures and 4 without. It was observed that all the mixtures specimens that were heated higher than 300°C, experienced a type of spalling and mass loss. In the tests, spalling ranged from insignificant aggregate spalling (which causes surface pitting) to, in extreme cases, large parts of the specimens being blown off with explosive force that are categorized in four types: explosive (parts larger than 1 cm), surface (parts smaller than 1 cm), aggregate and corner spalling.

The tests showed that the spalling degree decreased drastically when the water to binder ratio levels increased in the mixtures containing silica fume and also that silica fume in general could control explosive spalling due to increasing tensile strength.

3.3.0.3 Self compating concrete (SCC)

Tests ran by [Mathew and Paul, 2011] on SCC concluded that explosive spalling occurs in both vibrated concrete and SCC in the temperature range between 350°C and 580°C. On the other hand, no spalling was observed in any of the LSCC (Laterized Self Compacting Concrete) specimen tested. No crack was found in LSCC up to 600°C. Surface cracks were found on the specimens only at 800°C and the number of cracks was more in water cooled specimen.

3.3.1 Overview

As an overview of the experimental results on different types of concrete, it can be stated that the main factors contributing to spalling are the aggregate mixt and water to cement ratio (the heating rate was the same as they all used the standard ISO 834 Fire).

Related to aggregates, addition of silica fume can be a parameter that controls the likelihood of spalling due to increasing of tensile strength of concrete. Great results of using Laterized Self Compacting Concrete show that this replacement of the traditional aggregates could be considered as a substitute fire protection material for conventional concrete.

It is interesting to analyze the results when it comes to water to binder ratio on HSC. It is stated that low water to binder ratios have greater susceptibility to spalling because of the very dense concrete obtained with silica fume as a cement replacement. Even though low ratio implies higher strength and lower porosity, this will lead to higher pressures in the material. This is the opposite as for the normal concrete, where it is considered that spalling will not occur for moisture content lower than 3%.

It is clear that there is a large difference between normal concrete and the newly developed concretes because of the thermodynamic conditions met in the porous network of the latter, which results in a much high pore pressure that increases the changes of spalling occurrence.

For a better understanding of the features that can induce spalling, one should have knowledge about concrete characteristics at high temperatures. In the following, these will be exposed and analyzed based on experimental work.

CHAPTER 4

Concrete Behavior at Elevated Temperatures

This chapter begins with a brief description of what happens with a concrete member as the temperature increases within. After this thermal properties (density, specific heat and conductivity) influencing concrete behavior during fire are explained, along with hygral properties (moisture content, vapor pressure, permeability, porosity) as well as mechanical properties.

4.1 Temperature Effects on Chemical Composition

Concrete is a composite construction material consisting generally of mineral aggregate, cement and water. Cement and water together create the cement paste that glues the aggregates and fills the voids within. The microstructure of the concrete, depending on different ratios of water/cement can be seen in figure 4.1.

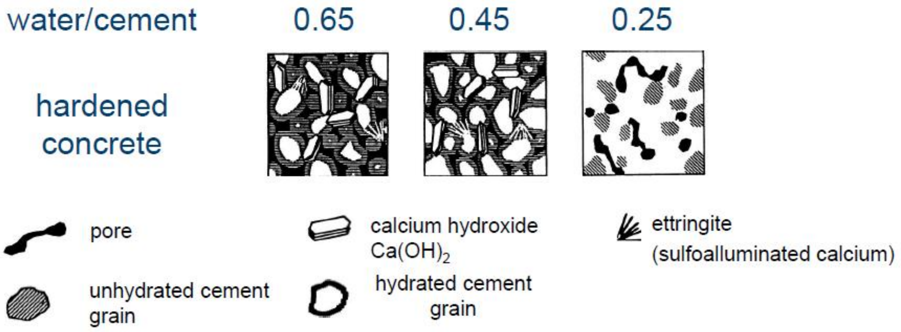

Figure 4.1. Microstructure of concrete [Aïtcin and Neville, 1993]

Concrete exposed to fire experiences chemical decomposition, depending on the temperature. The different chemical reactions that follow this process will not be explained in detail, because this is not the interest of this thesis. Instead, to have a general idea, a simpler explanation will be given regarding of what happens in the concrete with growing temperature following figure 4.2 and explanations given by [Bažant and Kaplan, 1996], [Aïtcin and Neville, 1993]:

- *Above* 100° *C:* There is an insignificant weight loss due to expulsion of evaporable water from hardened cement paste and aggregate.

- 100° *C to* 200° *C:* Occurrence of vapor pressure in the micro pores and continuance of weight loss due to evaporation of water. Dehydration of cement gel begins at around 180°C.

- 200° *C to* 500° *C:* Weight loss increase mainly due to the loss of water from gel pores as well as the first stage of dehydration and breakdown of tobermorite gel occurs. Above 450°C the portlandite $Ca(OH)_2$ dissociates into calcium oxide CaO and water H_2O.

- 500° *C to* 700° *C:* The rate of weight loss keeps increasing because of decomposition of calcium hydroxide in cement paste and decomposition of CSH (calcium silicate hydrate) phases. This is followed by the formation of $\beta - C_2S$ (quartz silica). From 700°C the concrete desegregations starts.

- 700° *C to* 900° *C:* Decarbonation of calcium carbonate in the limestone aggregate concrete, which occurs at about 800°C.

- *Above* 900° *C:* Melting of cement paste and aggregate at 1150°C and 1200°C. No further measurable weight loss. At 1270°C limestone aggregate concrete consists mostly of white porous calcium oxide. Glassy phase of basalt, quartzite and limestone concrete.

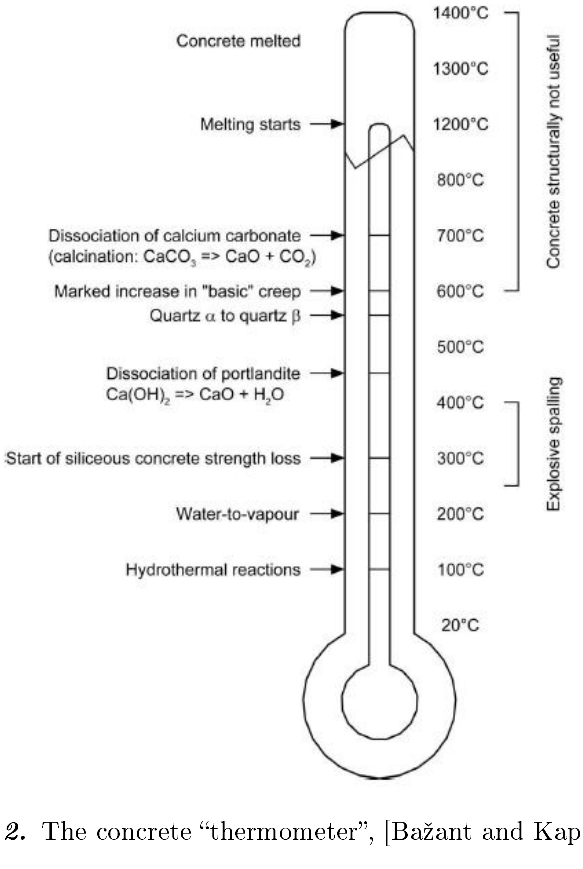

Figure 4.2. The concrete "thermometer", [Bažant and Kaplan, 1996]

4.2 Thermal Properties

Thermal properties of concrete refer to density, thermal conductivity and specific heat. This parameters have a significant influence on the temperature distribution within a concrete member exposed to fire and therefore will be explain in the following.

4.2.1 Density

The density of a material, ρ measured in kg/m^3 represents the ratio between its mass and its volume.

According to [Buchanan, 2001] density of concrete does not change much with increasing temperature. The only change it goes through is a reduction of approximately $100kg/m^3$ due to evaporation of free water, which has minor effect on thermal response. Density varies according to type of concrete: 'dense' concrete has a density of about $2400kg/m^3$ whereas lightweight concrete has a reduced density of $1750kg/m^3$. There is an exception, in case of limestone (calcareous) aggregate concrete that decomposes above 800°C with a corresponding decrease in density.

4.2.2 Thermal conductivity

The thermal conductivity, k [W/mK] is defined as the property of a material to conduct heat or the rate transmitted through a unit thickness of material per unit temperature difference.

The low thermal conductivity, among other properties, gives concrete a good behavior in fire. Thermal conductivity varies depending on aggregate, moisture content (increases with increase water content) and cement paste (low cement contends have a higher conductivity),[Buchanan, 2001].

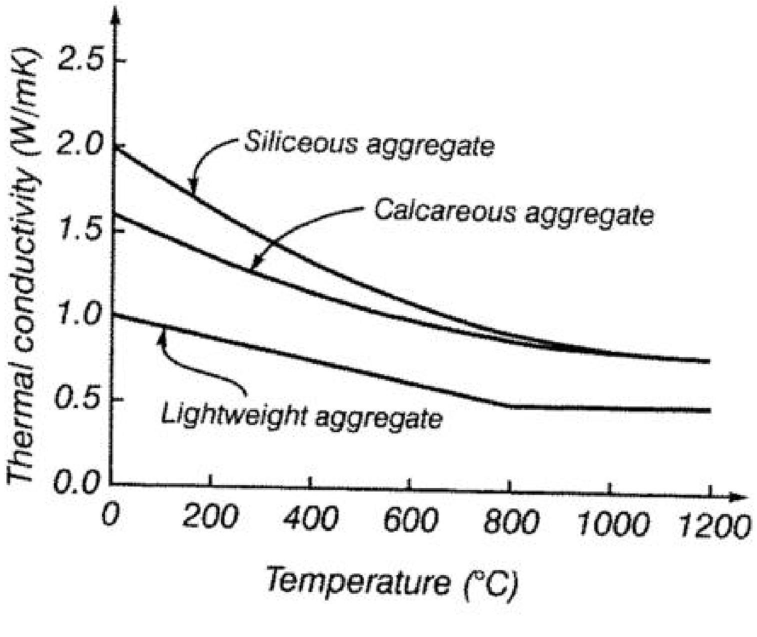

Figure 4.3. Thermal conductivity of concrete [EC2-EN1992-1-2, 2005]

When the concrete contains highly crystalline rocks such as quartzite, the thermal conductivity is relatively high. These values decreases as the temperature increases. When dealing with aggregates derived from amorphous rock formation such as basalt and dolerite, thermal conductivity is low. Lightweight aggregates have much lower conductivity (around $0.8W/mK$) due to their porosity, [Bažant and Kaplan, 1996]. Figure 4.3 illustrates this idea.

4.2.3 Specific heat

By specific heat, c_p $[W/mK]$, one refers to the energy required to heat up with one degree a unit mass of material.

The specific heat of concrete depends on aggregate and moisture content. Figure 4.4 shows the trend of the specific heat for concrete with siliceous or calcareous aggregates with different moisture content. Between 100°C and 200°C a peak can be noticed that is due to the water being driven off from the concrete during the heating process. Approximate design values are $1000J/kgK$ for siliceous and calcareous aggregate concrete, and $840J/kgK$ for lightweight concrete, [EC2-EN1992-1-2, 2005].

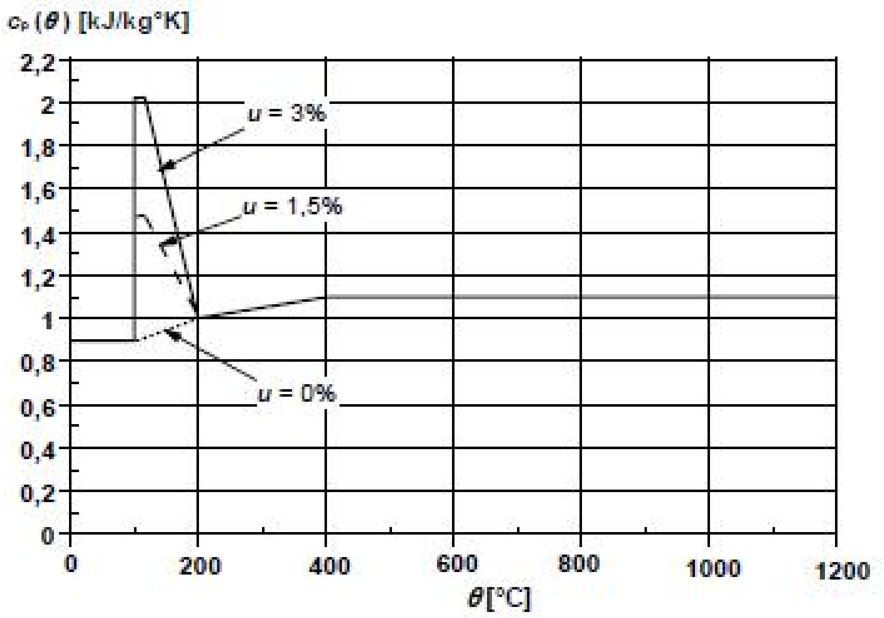

Figure 4.4. Specific heat of concrete [EC2-EN1992-1-2, 2005]

4.3 Hygral properties

The hygral properties refers, in a large extend to the moisture diffusion, pore pressure, permeability and porosity. Depending on the author, these properties are sometimes defined as physical or even thermal characteristics.

4.3.1 Moisture Content and Vapor Pressure

Bažant and Kaplan [1996] states that moisture content of concrete at elevated temperatures is affected by size and shape of the concrete member, rate and period of heating, and environmental conditions. In turn, moisture content affects properties such as shrinkage, density, deformation under load, creep and thermal conductivity, which influences thermal gradients and consequently thermal stresses. The thermodynamic of the system is disturbed by the water near the surface that tends to evaporate first. This moisture transfer continues until equilibrium is reached.

Moisture transfer in concrete can be done by diffusion, consisting of a flux due to gradient of moisture concentration or gradient of temperature. The difusivity increases as temperature increases. At temperatures above 100°C, the temperature gradient can be disregarded and the moisture flux can be considered to be transported by pore pressure gradient.

The pore pressures or vapor pressures are function of temperature and of the pore size of the specimen. An example of pore pressure data for heated concrete can be seen in figure 4.5. Knowledge about permeability and water diffusion is required for calculation of transient pore pressure in heated concrete.

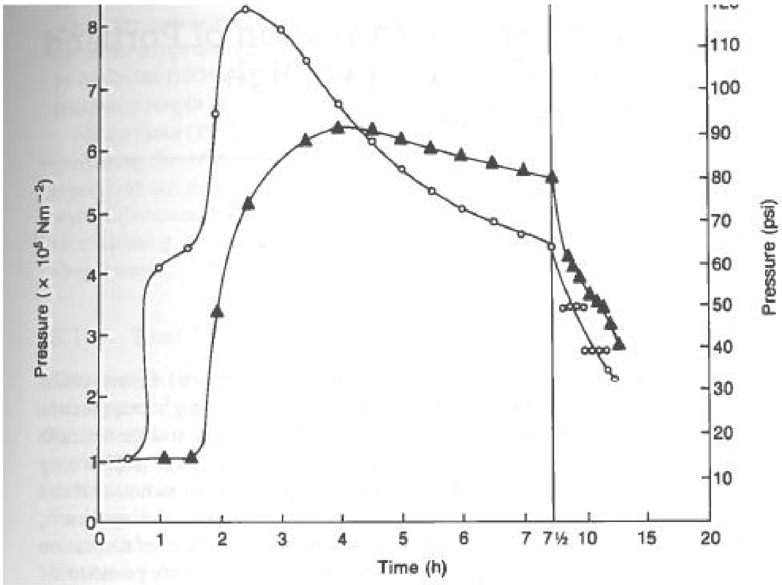

Figure 4.5. Vapor pressure data for heated concrete wall [Bažant and Kaplan, 1996]

4.3.2 Porosity and permeability

4.3.2.1 Porosity

By porosity one understands the ratio of pore volume to its total volume.
Results from tests conducted on cylindrical mortar specimens made with Portland and blast furnance slag cement were collected in [Bažant and Kaplan, 1996]. From this it can be reported that gradual heating causes changes in the distribution of pore structure: the total pore volume increased and the distribution of pore sizes was affected. The relatively small changes in pore volume on heating to 300°C was considered due to structural changes

resulting from dehydration processes occurring mainly in pores of small size which could not be determined with the mercury porosimetry method. The significant increase in total pore volume caused by heating to 600°C was probably due to an expansion of the pores or the formation of micro cracks. Heating up to 900°C resulted in further increase in pore volume.

Further tests investigation concluded that the porosity of unloaded heated specimens increased more than when heated under load. Concrete that was cooled after heating and then stored in air in the laboratory did not tend to re-establish lower porosity, Bažant and Kaplan [1996]. Figure 4.6 indicates a significant increase of porosity in the range of critical temperature. At 1000°C a decrease can be noticed due to formation of ceramic bounding. Line a) represents concrete made with Portland cement, b) with blast-furnace cement and chamotte and c) blast-furnace cement, chamotte and clay.

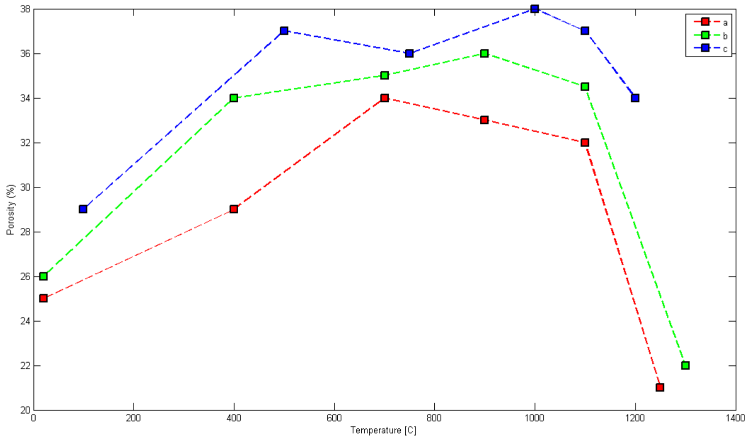

Figure 4.6. Porosity of concretes made with different types of cement [Bažant and Kaplan, 1996]

4.3.2.2 Permeability

Permeability represents the rate of flow of a fluid/gas into a porous solid. The permeability depends on the porosity, it increases with increase in the average pore size and also on the type of aggregate. Another way of increasing the permeability is the formation of by microcracking caused from the sudden change of phase of liquid water into steams. Permeability is expressed through intrinsic permeability and relative permability. Compared to normal concrete, HPC or HSC have lower permeabilities. Up until now, measurements of permeability are conducted at room temperature and few information is available on permeability of HPC at elevated temperatures, [BOŠNJAK et al., 2010].

4.4 Mechanical Properties

4.4.1 Compressive Strength

The assessment of the compressive strength will be illustrated based on the experimental tests and research work of [Hertz, 2005]. It is stated that due to the fact that concrete heated to less than 300°C can recover after a fire by absorbing moisture from the air, but when the micro cracks are formed the strength loss is permanent and the residual strength is smaller.

Figure 4.7 shows the compressive strength for siliceous concretes. The property ξ_{cc} is given as the ratio between the HOT (during fire) average strength at the test and the original average strength at 20°C. In 4.7(a), the limits of the band are shown as dotted lines, and a full drawn design curve is made as an average of the curves. The curves are valid for unloaded concrete. The CEN curve represents a transient curve from *ENV 1992-1-2. Design of Concrete Structures; General Rules, Structural Fire Design.*
In figure 4.7(b), curves are given for a residual COLD (cooling phase) condition after a fire based on 12 test series. As seen the relative residual strength ξ_{cc} is about 0.20 smaller than the HOT strength for temperatures above 400°C.

When testing lightweight concrete, the differences between HOT and COLD were smaller than in the previous case because of little thermal expansion and therefore only slight damage to the concrete, and at the same time, ensuring small thermal conductivity.

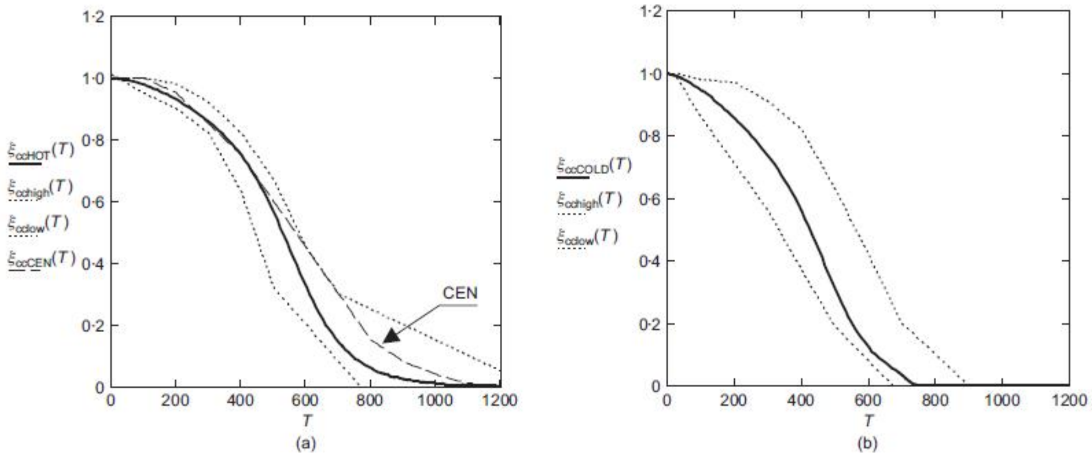

Figure 4.7. Compressive strength of siliceous concrete in (a) a HOT and (b) a residual COLD condition [Hertz, 2005]

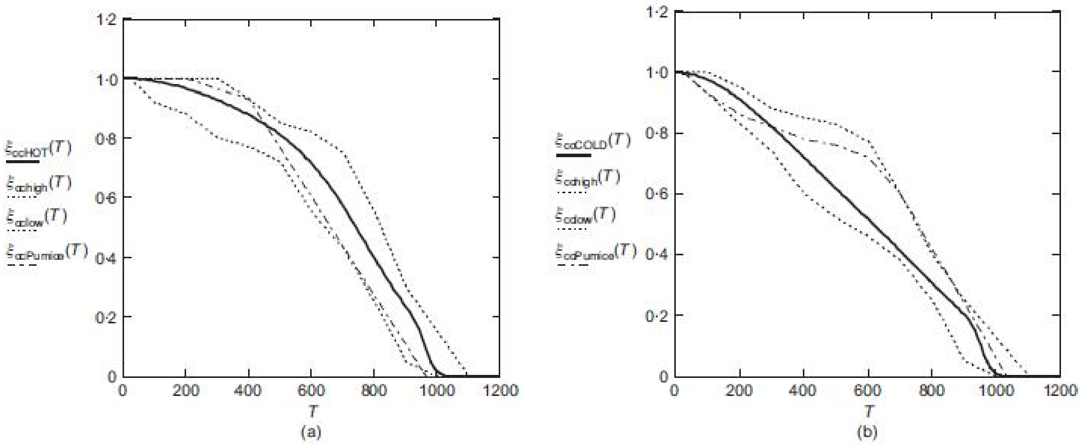

Figure 4.8. Compressive strength of lightweight aggregate (expanded clay) concrete in (a) a HOT and (b) a COLD condition. Pumice is a natural aggregate [Hertz, 2005]

It can be concluded that compressive strength depends on the aggregate type, does not depend on water/cement ratio during a fire down to a value of approximately 0.40 because excessive water evaporates. For lower values, unhydrated cement may act as fire-resistant filler, which can reduce the strength loss. [Hertz, 2005] also concludes that age of the concrete has no influence except for fresh concrete where heating will give a forced hydration within the first 150°C before the concrete is damaged. This may cause a slight increase of the compressive strength, and the following damages must be assessed related to this increased final strength level.

4.4.2 Tensile strength

According to [EC2-EN1992-1-2, 2005] tensile strength of concrete should normally be ignored as a conservative measure. As seen from figure 4.9 tensile strength also reduces with increasing temperature, the reduction already taking place at 100°C. The reduction of the characteristic tensile strength of concrete is represented by the coefficient $k_{c,t(\theta)}$ which denotes the ratio between the tensile strength at room temperature and the one at elevated temperatures.

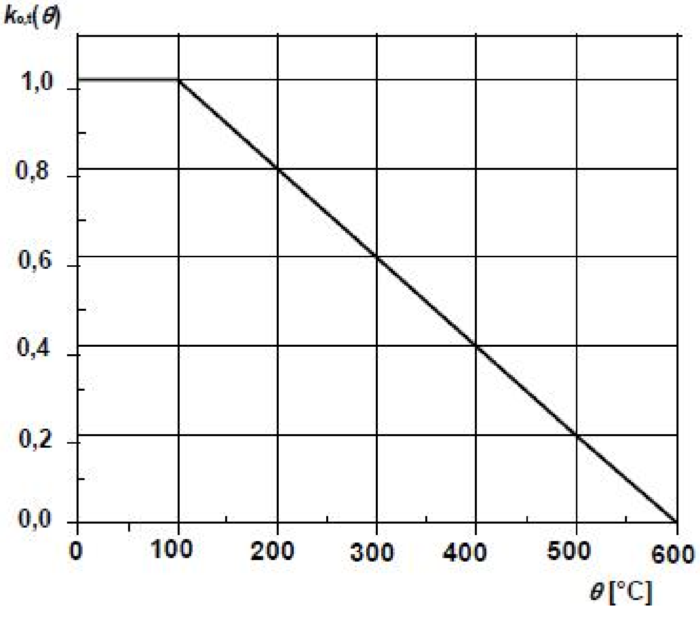

Figure 4.9. Tensile strength at elevated temperatus [EC2-EN1992-1-2, 2005]

4.4.3 Modulus of Elasticity and Poisson's Ratio

4.4.3.1 Modulus of Elasticity

Studies carried out and assessed by [du Bèton, 2008] show that modulus of elasticity depends mainly on the compressive strength of the concrete. Therefore, Young's modulus is affected by the same factors as the compressive strength, like type of cement, water cement ratio, type of aggregate, loading conditions during the thermal cycle, maximum temperature reached during heating. However, besides the last parameter, only the type of aggregate and to a lesser extent the loading conditions during heating process have a sizeable influence on the elastic modulus, which is more temperature- sensitive than the compressive strength (both at high temperature and after cooling), because concrete stiffness is directly affected by thermal cracking.

As seen in figure 4.10, for siliceous aggregates like basalt and quartzite, $E_c^T/E_c^{20} = 0.4 - 0.5$ at 500°C, while for light-weight aggregates are close to or better than calcareous aggregates (at 500°C, E_c^T/E_c^{20} up to $0.70 - 0.75$ for expanded clay).

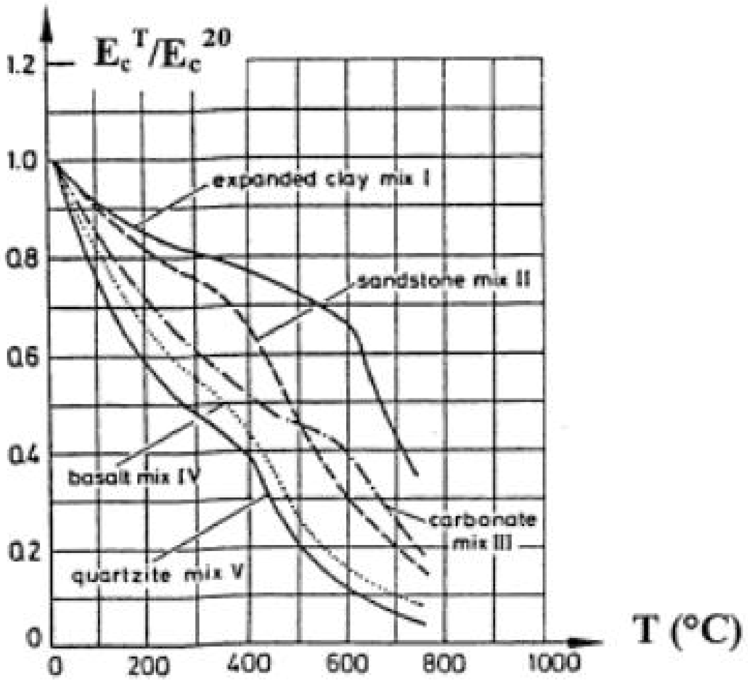

Figure 4.10. Elastic moduli of similar mixes containing different type of aggregate [du Bèton, 2008]

4.4.3.2 Poisson's Ratio

As for the Poisson's ratio, it is generally evaluated by measuring the transverse strains in a specimen loaded in uniaxial compression, but can also be estimated from the elastic and shear moduli.
There is still few data on this parameter so far. Test conducted by [Bažant and Kaplan, 1996] show that in the case of siliceous aggregates the Poisson's ratio tends to decrease with the temperature, with no significant differences between the high-temperature and the residual values above 100°C ($\nu_c = 0.23 - 0.10$, with 0.10 both at 400°C and after cooling. However, other results indicate a completely contrary trend for both siliceous and calcareous mixes (up to 0.23 at 400°C), with a dependency on the temperature for light-weight mixes.

4.4.4 Components of Strain

The deformation of concrete is usually described by assuming that the total strain ε consists of four components being, [Buchanan, 2001]:

$$\varepsilon = \varepsilon_{th}(T) + \varepsilon_{\sigma}(\sigma,T) + \varepsilon_{cr}(\sigma,T,t) + \varepsilon_{tr}(\sigma,T) \tag{4.1}$$

$\varepsilon_{th}(T)$ is the thermal strain being a function only of temperature,T,$\varepsilon_{\sigma}(\sigma,T)$ is the stress related strain, being a function of both the applied stress σ and the temperature, $\varepsilon_{cr}(\sigma,T,t)$ is the creep strain, being also a function of time,t, and $\varepsilon_{tr}(\sigma,T)$ is the transient strain, being a function of both the applied stress and the temperature.

4.4.5 Stress- Strain Relation

The stress-strain relationship for concrete at elevated temperatures can be seen in figure 4.11. It includes elastic and plastic components of strain resulting from applied stresses. The ultimate compressive strength drops, and the strain at peak stress increases with increasing temperature. The main factor influencing the stress-strain behavior of concrete during fire is the type of aggregate. Other factors are the aggregate cement ratio, loading of the concrete and of course temperature.

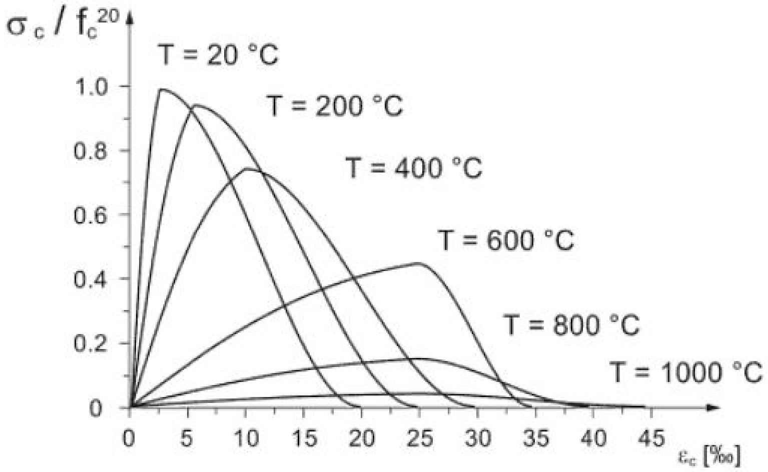

Figure 4.11. Stress-strain curves for concrete at high temperatures [EC2-EN1992-1-2, 2005]

The main factor influencing the stress-strain behaviour of concrete during fire is the type of aggregate. Other factors are the aggregate cement ratio, loading of the concrete and of course temperature.

4.5 Summary

As a conclusion to the before presented properties it can be noticed that concrete behavior at elevated temperatures varies depending on many parameters such as the concrete type (lightweight concrete, normal or "new" concrete), aggregate type, moisture content, cement paste, size and shape of the member, water cement ratio, heating rate, type of concrete, permeability, etc.

In order to assess the risk of spalling, models can be built based on the concrete comportment at elevated temperatures. The models can be simple ones, starting from a physical one, then a mathematical one and a more complex one, the numerical model, as presented in figure 4.12. The models are connected in the way that for having understanding about the complicated model, one should start with a basic one, the physical model and then continue, as indicated by the arrows.

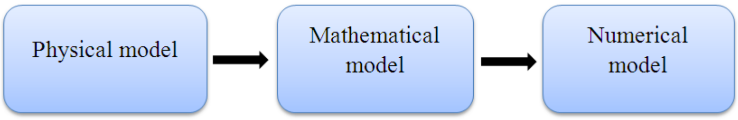

Figure 4.12. Different models to illustrate spalling

Chapter 5

Physical Model

In this chapter a physical model will be exposed based on the previous presented information regarding the spalling process and concrete behaviour at elevated temperatures. Close account will be given to temperature, moisture, vapor pressure and stress state in the element. The physical model can be considered as the sum of a thermo-hygral model and a mechanical model. In the end, a conclusion will be made.

5.1 Critical factors

Even though in chapter 3, three different types of spalling failure were exposed, the present physical model considers only spalling due to vapor pressure and the one due to restrain thermal dilatation (thermal stress spalling). The thermal crack spalling can be considered as included in both modeles because they both take into account the temperature gradient and decomposition of hydratation.

As presented in the preceding chapters, there are several parameters that contribute to the spalling phenomenon. For building up a model that can be applied to a larger extend, independent on some parameters such as composition and structure of the cement paste, mix design, aggregate type, water to cement ratio, etc., focus will be given on four critical factors: temperature, moisture, vapor pressure and stress state.

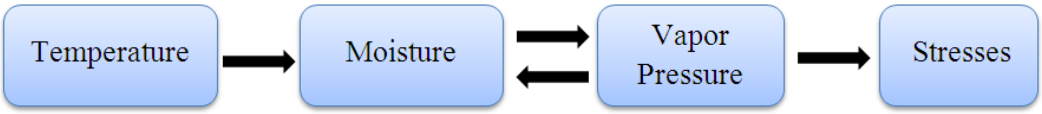

Figure 5.1. Crucial factors inducing spalling

As seen in figure 5.1 the temperature is the starting point. This will affect the water content of the member. The water will tend to evaporate and will suffer a phase change, transforming into steams. The direction of the arrows between moisture and vapor is in both sides because when the vapors travelling towards the core of the element meet temperatures lower than 100°C they transform back into water. The pressure build up inside the constituent will generate an increase of the tensile stresses, that, as a result will generate cracks. Depending on the severity of the cracks and temperatures, local, progressive or explosive spalling might occur.

5.2 Role of the crucial factors

Having depiction 5.1 in mind, a physical model of concrete spalling can be illustrated starting from explaining the role of each key parameter involved. These parameters cannot be considered separately, as their influence is approximately the same in the spalling process and also they are closely linked together. The next subsections will describe their contribution to the concrete behavior at high temperatures.

5.2.1 Temperature

As exposed to only one side, the temperature at the exposed side will be high (can reach approximated temperatures of 1000°C to 1200°C) and then it will decrease along the element, dropping until the ambient temperature. This results in large temperature gradients within, depending on the heating rate. For fast heating rates, the gradient will be higher and for slow heating rates, the gradients will have minor values. As a consequence, the stress state inside the member will go through changes. The heated surface will suffer a thermal restrain and the surface beneath it a thermal expansion. This will generate compression stresses at the surface layer and tension stresses inside. These stresses will have influence on the crack formation that further on will increase the permeability of the concrete near the surface. On the other hand, this will make it easier for the vapors to escape outside.

In this stage the temperature is not the only ones responsible for the before described process. The developed stresses are also due to evaporation of moisture. This type of spalling occurrence was described previously in section 3.2.2.2 as thermal stress spalling.

5.2.2 Moisture content

The temperature increase will obviously stimulate the moisture content. A gradual loss of the evaporable water will occur near the heated part, depending on the heating rate and porosity of material, (porosity is increasing along with the temperature). This water content will go through a phase change, transforming into vapors at temperatures above 100°C and will coincide with a dehydration of the surface concrete member, forming the so called dry zone. Advancing further in the element, a quasi-dehydrated zone will be found and then a wet one (conditions met before fire exposure). Consequently of the dehydrated zone, the permeability of the surface layer will increase and cracks will be formed, their severity depending on the material properties. This fact will again make it easier for vapors to escape and therefore decrease the vapor pressure inside. Because of this, also the tensile stresses inside will be lower. But even so, the damage provided by the cracks can be serious enough.

5.2.3 Vapor pressure

As moisture starts boiling and changes into vapor, a part of it escapes through the concrete pores and the other part is driven inside the member forming a saturated front. The permeability of the material influences the vapor travel and therefore the pressure gradient. Higher permeabilities will induce a lower pressure gradient and more vapors can escape, meanwhile low permeabilities will act as a barrier for the vapors, ending in a high pressure gradient.

Within the moisture clog or saturated front, the vapor pressure reaches its peak. Here also moisture along with vapors is present. In this area the relative humidity is increased above its initial value.

The vapor pressure developed here has a significant importance on the stress state, increasing the tensile stresses inside and as a result cracks will develop, leading to a strength reduction of the material that can eventually conduct to collapse of the member. This type of failure was depicted as pore pressure spalling.

5.2.4 Stress development

The tensile stress development is related to the temperature distribution that is non-uniform and the compression stresses to the moisture (removed by thermal means) distribution that as well is non-uniform. Also the gas pressure increases the tensile stresses having a noticeable influence and generating cracks that will promote along the surface layer.

5.3 Physical model

It cannot be stated that a single factor alone among the four mentioned has such a stronger effect that can lead to explosive spalling. Therefore the before presented parameters should not be considered as independent, but closely connected. Even though some researchers state that the main reason for explosive spalling is the vapor pressure(when the tensile stress generated by the vapor pressure exceeds the tensile strength of the concrete explosive spalling occurs) in the present physical model this assumption is not valid. All the factors are strongly connected and summing them up can end into significant outcomes.

Based on the crucial factors involved, the physical model can be a divided in a thermo-hygral model and a mechanical model as presented in the above scheme.

The thermo-hygral model contains the mass transport of liquid phases of course with temperature included. The main physical phenomena will be liquid water flow because of pressure gradients and capillary effect, gas pressure, evaporation and dehydration.

The mechanical model will be done by an elastic stress/strain relationship coupled with the influence of temperature and moisture on the concrete element.

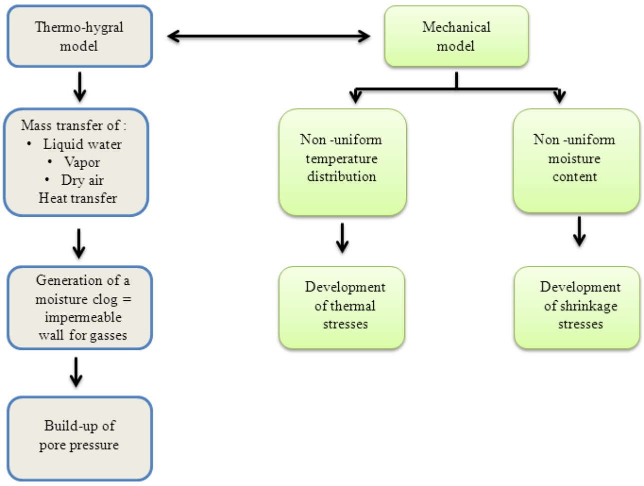

Figure 5.2. Thermo-hygral model and mechanil model

A more illustrative example of the thermo-hygral and mechanical models can be seen in the next figures.

Figure 5.3 shows the temperature distribution, the moisture clog and vapor pressure as a result of heat and mass transport. As the temperature increases triggers a moisture and vapor concentration in the drying zone that will form an impermeable wall stopping any further transport.

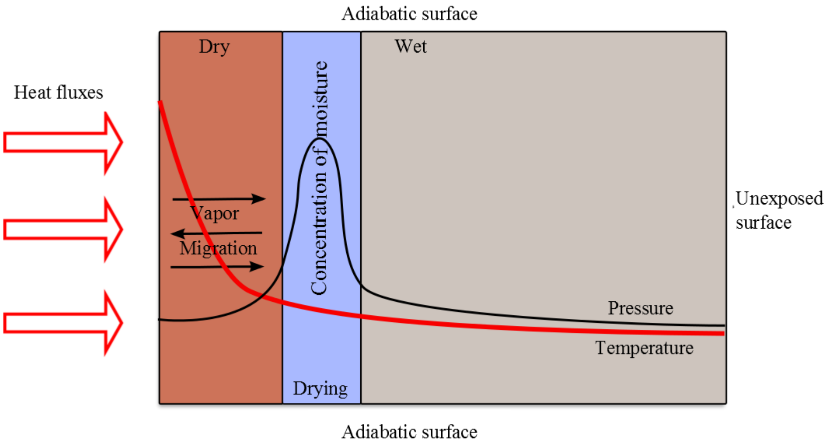

Figure 5.3. Connection between parameters involving spalling

Regarding stress development, in the dry zone the cement paste shrinks with water escape, resulting in a compression stress state and the aggregates dilate (tension stress state). The vapor driven by pressure gradients will trigger in turn tensile stresses, effect presented in figure 5.4.

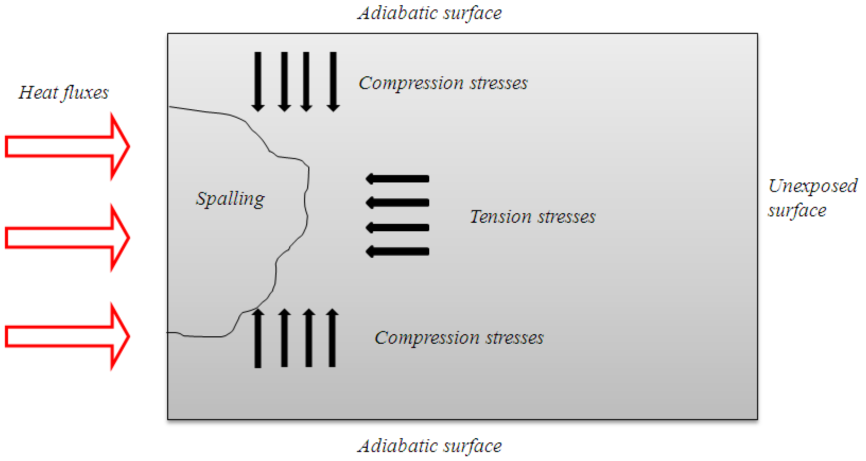

Figure 5.4. Stress state inside the concrete member exposed to fire

5.4 Summing up

Therefore, spalling is a complex phenomenon that is a result of the interconnection between main parameters such as temperature, moisture content, vapor pressure and stresses. A big influence on spalling has the heating rate, that is of course connected to the temperature. A fast heating rate can severely damage the member and trigger accelerated moisture loss and high pressure gradients that will generated increased tensile and compression stresses. In conclusion, same importance should be given to each of the exposed factors and any model trying to model spalling should definetly account for all of them.

Having as a starting point this physical model, more complex and complicated models can further on be implemented.

Chapter 6

Mathematical Model

The principal transport equations refer to the formulation used to analyze the 1-D model of a concrete element exposed to fire requiring for the temperature, the liquid water, vapor and dry air transfer. The equations will be explained along with the terms contained by them. Brief description of the water species in concrete will be given. The conservation equations will be exposed. Different expressions for thermal dilatation strain, shrinkage, thermo-chemical and transient thermal strain are given. In the end formulas for the effective stress can be seen.

6.1 Principal transport equations

6.1.1 Heat transfer

The temperature is transferred through the element, from high temperature-region to low temperature-region by conduction. This phenomenon can be expressed by *Fourier's heat conduction law*, which is given by expression 6.1. The negative sign indicates that heat is transported in the direction of decreasing temperature. If the temperature is independent of time, the problem is a simple one and solving equation 6.1 is enough to find the desired quantity of the heat flux.

$$q = -kA\frac{\partial T}{\partial x} \tag{6.1}$$

where:

A	area $[m^2]$
k	thermal conductivity of concrete [W/m°C]
T	temperature in the concrete at distance x inside the element [°C]
q	conduction heat flux $[W/m^2]$
$\frac{\partial T}{\partial x}$	temperature gradient in the direction of the heat flow

When the temperature is dependent of time, the situation becomes more complex. In this case, the temperature profile in the concrete can be expressed by equation 6.2:

$$\rho c\frac{\partial T}{\partial t} = \frac{\partial}{\partial x}(k\frac{\partial T}{\partial x}) \tag{6.2}$$

Where:

ρ	density $[kg/m^3]$
c	specific heat $[J/kg$°C]
t	time $[s]$

The thermal properties involved in the before presented equations were considered as follows, [Benes and Mayer, 2007], in the case of temperature dependent parameters:

$$k(T) = 1.67 - 5 \cdot 10^{-4}(T - 293.15) \tag{6.3}$$

$$(\rho c)(T) = 2434600 - 3.4 \cdot 10^{-4}(T - 293.15) \tag{6.4}$$

A second case was considered with constant density and thermal conductivity, but temperature dependent specific heat according to [EC2-EN1992-1-2, 2005]:

- $c = 900 J/kgK$ $20° C < T < 100° C$
- $c = 900 + (T - 100) J/kgK$ $100° C < T < 200° C$
- $c = 1000 + (T - 200) J/kgK$ $200° C < T < 400° C$
- $c = 1100 J/kgK$ $400° C < T < 1200° C$

6.1.2 Water species

As presented in chapter 4, concrete is a porous material composed of cement paste and aggregates. The water contained by the element is divided in water that is bounded to the cement as chemically adsorbed water and water contained by the pores in liquid and in vapor form. These are illustrated in figure 6.1. The one that will suffer changes during the heating process is the water contained by the pores and the chemically adsorbed water contained by the cement paste (at higher temperatures it will be released by dehydration and it will evaporate).

As seen, the liquid phase is composed of physically bound water in form of gel water and capillary water as free water. The mixture is available for temperatures lower than the critical temperature of the water $T_{cr} = 374.15$°C. This point represents a phase where no boundaries exist, where there is no distinction between liquid and vapors. When exceeding this temperature, the liquid phase will contain bound water only. The gas phase has the same components, dry air and water vapor during the whole process.

The dehydration process of the concrete takes place for temperature exceeding 105°C. The value of 105°C is also a representative one, as the free water and the physically bound water will evaporate at this temperature.

At temperatures lower than 100°C the water flow is driven by moisture concentration gradient and at temperatures above 100°C the transport takes place in vaporized state as steam and is driven by pore pressure gradient.

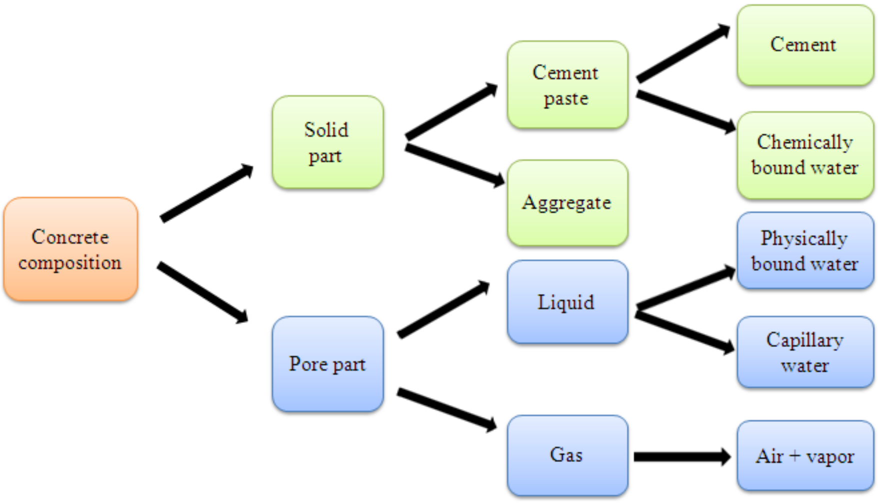

Figure 6.1. Concrete composition as a porous material

The following equations will describe the mathematical definition of the water contained by the pores as liquid and gas form. Therefore, the transport equations will regard liquid water, dry air and vapor water transport that are carried out by diffusion.

6.1.3 Moisture distribution

The moisture state refers to the sum of water vapor and liquid water. It can be described in terms of evaporable or free water or relative humidity, [Bažant and Kaplan, 1996], but in zones with fully saturated liquid state, where pressures higher than the atmospherical pressure occur, there are some mismatches and the moisture state can be modeled using the capillary pressure, [Gawin et al., 2002]. The *Kelvin equation* expressed the equilibrium state of the capillary water:

$$p^c = -\rho^w \frac{RT}{M_w} ln(\frac{p^{gw}}{p^{gws}}) \tag{6.5}$$

Where:

p^c	capillary pressure $[Pa]$
ρ^w	water density $[kg/m^3]$
R	universal gas constant $[J/molK]$
M_w	molar mass of water vapor $[kg/kmol]$
p^{gw}	water vapor pressure $[Pa]$
p^{gws}	water saturation pressure $[Pa]$

The relative humidity, RH represents the ratio between the water vapor pressure and the water saturation pressure:

$$RH = \frac{p^{gw}}{p^{gws}} = exp(\frac{p^c \cdot M_w}{\rho^w \cdot T \cdot R}) \tag{6.6}$$

Where $M_w[kg/mol]$ is the molecular mass of water wapor and $R = 8.314[J/molK]$ is the gas constant.

The water vapor saturation pressure p^{gws} has the following expression for T in [K]:

$$p_{qws}(T) = exp(23.5771 - \frac{4042.9}{(T - 37.58)}) \tag{6.7}$$

As presented before there is no capillary water in the pores above $T_{cr} = 374.15°\text{C}$, therefore the capillary pressure can be treated formally as water potential multiplied by the density of liquid water, see expression 6.8.
Also $p^c = p^g - p^w$ and after the critical point is reached, $p^g = p^w$, where p^g $[Pa]$represents the total gas pressure and p^w $[Pa]$ the water pressure. The total gass pressure is the sum of water vapor pressure and dry air pressure: $p^g = p^v + p^a$.

$$p^c = -\Psi_c \rho^w(T_{cr}) \tag{6.8}$$

The water density for T in [K] :

$$\rho^w = 999.84 \cdot [1 - 6.8 \cdot 10^{-5}(T - 293.15)] \tag{6.9}$$

The moisture transport can be expressed by *Darcy's law*, in terms of porosity:

$$J_w = \phi S_w \rho^w v^w \tag{6.10}$$

Where:

J_w	liquid water flux [m/s]
ϕ	porosity [-]
S_w	degree of saturation with liquid water [-]
v^w	velocity of liquid phase [m/s]

The degree of saturation with liquid water, which is assumed to be constant in the capillary moisture range:

$$S_w = [1 + (\frac{p^c}{p^c_b})^{10}]^{-0.26} \tag{6.11}$$

In terms of permeability again *Darcy's law* is applied. The liquid water flux and the vapor water flux are:

$$J_w = -\rho^w \frac{kk_{rw}}{\mu_w} \frac{\partial p^c}{\partial x} \tag{6.12}$$

$$J_v = -\rho^v \frac{kk_{rv}}{\mu_v} \frac{\partial p^v}{\partial x} \tag{6.13}$$

Where:

k	intrinsec permeability
k_{rw}	water relative permeability [-]
k_{rv}	water vapor relative permeability [-]
μ_w	dynamic viscosity of water
μ_v	dynamic viscosity of water vapor

The expressions for the intrinsic permeability, water permeability and gas relative permeability can be seen below, [Benes and Mayer, 2007]:

$$k = 10^{-20} \cdot 10^{0.005(T-273.15)\cdot(\frac{p^g}{10125})^{0.368}} \tag{6.14}$$

$$k_{rw} = S_w^2 \tag{6.15}$$

$$k_{rv} = 1 - S_w \tag{6.16}$$

6.1.4 Pore pressure distribution

In order to model the transport of the water vapor some assumptions need to be considered: the flow takes place mainly in the largest pores of the element and the vapors behave as an ideal gas, being a sum of water vapor and dry air. Therefore the gas flow can be expressed using *Darcy's law* as follows:

$$J_{ga} = -\rho^v \frac{k k_{ra}}{\mu_{ga}} \frac{\partial p^g}{\partial x} \tag{6.17}$$

Where:

J_{ga}	dry air flux $[m^3/s]$
k_{rw}	relative permeability of the gas $[m^2]$
μ_{ga}	dynamic viscosity of dry air [Pa s]
$\frac{\partial p^g}{\partial x}$	gas pressure gradient [Pa/m]

The permeability k can be taken as a constant value whereas the dynamic viscosity of dry air μ is temperature [K] dependent:

$$\mu_{ga} = 17.17^10^{-16} + 4.73 \cdot 10^{-8}(T - 273.15) + 2.22 \cdot 10^{-11}(T - 273.15)^2 \tag{6.18}$$

6.2 Conservation equations

Conservation equations refer to the conservation equation of water species and energy conservation. The unknowns in the equations are the mass density concentration of liquid water, water wapor, dry air and the temperature.

6.2.1 Conservation equations of water species

Because of the different water species that coexist in concrete, there are also several different conservation equtaion of them: the liquid water, the water vapor and the dry air conservation equations. To be kept in mind that liquid water and water vapor are considered as one entity and that is moisture flux.

Conservation of liquid water:

$$\frac{\partial \eta^w \rho^w}{\partial t} + div(J_w) = -\dot{m_{vap}} \Delta H_{vap} + \dot{m_{dehydr}} \Delta H_{dehydr} \tag{6.19}$$

Conservation of water vapor:

$$\frac{\partial \eta^g \rho^v}{\partial t} + div(J_v) = -\dot{m_{vap}} \Delta H_{vap} \tag{6.20}$$

Conservation of dry air:

$$\frac{\partial \eta^g \rho^{ga}}{\partial t} + div(J_{ga}) = 0 \tag{6.21}$$

Where:

J_w	water flux $[m^3/s]$
J_{gw}	water vapor flux $[m^3/s]$
J_{ga}	dry air flux $[m^3/s]$
k_{rv}	relative permeability of the vapor $[m^2]$
ΔH_{vap}	enthaply of vaporization per unit mass [J/kg]
ΔH_{dehydr}	enthaply of dehydration per unit mass [J/kg]
$\dot{m_{vap}}$	rate of mass due to phase change $[kg/m^3 s]$
$\dot{m_{dehydr}}$	rate of mass due to dehydration $[kg/m^3 s]$

And $\eta_w = \phi S_w$, $\eta_g = \phi S_w = g$. S_w, S_g and ϕ denote the degree of water respectively the gas saturation and the porosity.
The enthalpy of evaporation can be approximated by *Watson formula*:

$$\Delta H(T) = 2.672 \cdot 10^5 (T_{cr} - T)^{0.38} \tag{6.22}$$

6.2.2 Energy conservation equation

The energy balance equation taking into account the conductive heat flow and the heat affecting the phase change and dehydration process can be expressed as an *Enthalpy balance equation of a multi-phase medium*, [D.Gawin et al., 2005] as seen in equation 6.23. The righ-hand side of the equation represents the energy needed for evaporation of liquid water and the one needed for evaporation of bound water by dehydration.

$$(\rho C_p)_{eff} \frac{\partial T}{\partial t} + (\rho_w C_p^w \mathbf{v}^w + \rho_g C_p^g \mathbf{v}^g) \cdot gradT - div(\chi_{eff} gradT) = -\dot{m_{vap}} \Delta H_{vap} + \dot{m_{dehydr}} \Delta H_{dehydr} \tag{6.23}$$

Where:

χ_{eff}	effective conductivity from experiments $[W/m$°C$]$
$(\rho C_p)_{eff} = \rho_s C_p^s + \rho_w C_p^w + \rho_g C_p^g$	[-]
C_p	effective specific heat of porous medium [J/kg °C]
C_p^g	specific heat of gas mixture [J/kg °C]
C_p^w	specific heat of liquid phase [Pa/m]
ρ_g	gas phase density $[kg/m^3]$
ρ_w	liquid phase density [kg/m^3]
ρ	aparent density of porous medium $[kg/m^3]$

The convection term $(\rho_w C_p^w \mathbf{v}^w + \rho_g C_p^g \mathbf{v}^g) \cdot gradT$ will be ingnored in further calculations considering the energy transfer by convection included in the thermal conductivity term. The final energy conservation equation is:

$$(\rho C_p)_{eff}\frac{\partial T}{\partial t} - div(\chi_{eff} gradT) = -\dot{m_{vap}}\Delta H_{vap} + \dot{m_{dehydr}}\Delta H_{dehydr} \tag{6.24}$$

By enthalpy one understands a thermodynamic property of a system equal to the sum of its internal energy and the product of the its pressure and volume, [Mifflin, 2006].

6.3 Modelling of stress and strains

High temperatures will induce stresses that together with the moisture change will produce damage in the form of local cracks that if further developed can lead to failure. It is important that the mathematical model takes into account parameters that vary with temperature, as well as factos that induce cracking and moisture change.

As presented in chapter 5, during the heating process, the cement paste shrinks with water escape, resulting in a compression stress state and the aggregates dilate progressing in a tension stress state. In other words, the shrinkage stresses develop due to a non-uniform distribution of moisture in the drying zone and the thermal stresses arise due to non-uniform temperature.
The total strain in the concrete was presented in chaper 4, in the *Mechanical Properties section* as being composed of the following:

$$\varepsilon_{tot} = \varepsilon_{th}(T) + \varepsilon_{el}(\sigma,T) + \varepsilon_{tchem}(V(T)) + \varepsilon_{tr}(\sigma,T) \tag{6.25}$$

Where:

$\varepsilon_{th}(T)$	thermal dilatation strain component [-]
$\varepsilon_{el}(\sigma,T)$	elastic strain due to effective stresses [-]
$\varepsilon_{tchem}(V(T))$	thermo-chemical strain (irreversible component) [-]
$\varepsilon_{tr}(\sigma,T)$	transient thermal strain(thermal creep) [-]

The shrinkage strain is included in the elastic strain due to action of capillarity pressure, [D.Gawin et al., 2005]. A detailed look will be given to the thermal dilatation strain, the shrinkage and thermo-chemical strain.

6.3.1 Thermal dilatation strain

The expression of the thermal dilatation strain is:

$$d\varepsilon_{th} = \beta_s(T)dT \tag{6.26}$$

Parameter $\beta_s(T)$ is the thermal dilatation coefficient that is linearly temperature dependent and it can be determined experimentally. Based on experimental work [Kaicheng et al., 2008] approximated a mathematical expression for the thermal dilatation coefficient:

$$\beta_s(T) = (0.008 \cdot \Delta T + 6) \cdot 10^{(-6)} \tag{6.27}$$

6.3.2 Shrinkage strain

The shrinkage strains are difficult to measure experimentally, therefore they will be computed based on the effective stresses. Equation 6.28 shows the effective stresses for material with small pores, [Gawin et al., 2004]:

$$\sigma^{''} = \sigma + \alpha \cdot p^s I \tag{6.28}$$

Where:

$\sigma^{''}$	effective Bishop stress tensor responsible for the skeleton deformation [Pa]
σ	Cauchy stress tensor [Pa]
$\alpha = 1 - \frac{K_T}{K_S}$	Biot coefficient [-]
K_S and K_T	bulk moduli for solid phase and the whole medium [Pa]
p^s	solid skeleton pressure [Pa]
I	unit tensor [-]

The solid skeleton pressure exerted by the liquid water and moist is:

$$p^s = p^g - x_s^{ws} p^c \tag{6.29}$$

Where:

p^g	pressure of gas phase [Pa]
x_s^{ws}	solid surface fraction in contact with the wetting water film [-]
p^c	capillary pressure[Pa]

Finally the increment of the shrinkage strains is:

$$d\varepsilon_{sh} = \frac{\alpha}{K_T}(dx_s^{ws} p^c + x_s^{ws} dp^c) I \tag{6.30}$$

The bulk modelus K_T depends on the temperature and on the damage parameter V. In equation 6.32 E_0 represents the Young's modulus of mechanically undamaged material [Pa] and T_a the ambient temperature.

$$K_T(T) = [1 - V(T)] K_T(T_a) \tag{6.31}$$

$$V(T) = 1 - \frac{E_0(T)}{E_0(T_a)} \tag{6.32}$$

The mathematical model for the shrinkage strains contains a lot of terms that are based on experimental work. Because of lack of experimental data, the model used in this thesis will be simplified. Following closely the thermal dilatation strain model, the shrinkage strain will be computed as seen in equation 6.33, where k_s $[m^3/kg]$ is the shrinkage coefficient and w $[kg/m^3]$ represents the loss in water content.

$$d\varepsilon_{sh} = k_s \cdot dw \tag{6.33}$$

The shrinkage coefficient k_s may be considered as approximately constant, $k_s = 10^{-5} m^3/kg$, [Bažant and Kaplan, 1996] and the loss in water content may be computed using the relative humidity RH and the sorption and desorption isotherms. In these isotherms usually the moisture content is given as a ratio between the moist mass of concrete and the mass of dry concrete.

6.3.3 Thermo-chemical strains

There is a lack of a theoretical model for the increment for the thermo-chemical strain due to the complicated physico-chemical nature of the phenomena, [Gawin et al., 2004]. A solution is approximated from direct experimental results:

$$d\varepsilon_{tchem} = d\varepsilon_{tot} - d\varepsilon_{sh} - d\varepsilon_{th} \tag{6.34}$$

Where $d\varepsilon_{tot}$ is an increment of the total experimentally measured strain and $d\varepsilon_{sh}$ and $d\varepsilon_{th}$ can be found based on the previous presented equations.

Because in the present case there were no available experimental data for computing the thermo-chemical strain, this will be not included in the further calculations.

6.3.4 Transient thermal strain

The transient thermal strain increment is obtained from:

$$d\varepsilon_{th} = \frac{\partial \overline{\varepsilon_{th}}(V)}{\partial V} \frac{\tilde{\sigma}}{f_c(T_a)} dV \tag{6.35}$$

The normalized thermal transient strain is computed from 6.36, where $\tilde{\sigma}$ is the "net" effective stress tensor and f_c the compressive strength of concrete[MPa].

$$\overline{\varepsilon_{th}}(V(T)) = [\varepsilon_{tot}(\tilde{\sigma},T) - \varepsilon_{tot}(0,T) - \frac{\varepsilon_{el}(\tilde{\sigma},T_a)}{1-V(T)}] \cdot \frac{f_c(T_a)}{\tilde{\sigma}(T)} \tag{6.36}$$

Again, also this strain component will be left out of further calculations. Due to the simplifications made, the total strain of concrete will be as seen in equation 6.37, a sum of the thermal, mechanical and hygral strain.

$$\varepsilon_{total} = \varepsilon_{th}(T) + \varepsilon_{el}(\sigma,T) + \varepsilon_{sh}(w,T) \tag{6.37}$$

6.3.5 Effective stress

Having the expressions for the strains, the effective stress σ is given by equation 6.38 where Λ_0 and represents the stiffness matrix of undamaged material [Pa].

$$\sigma'' = (1-d)(1-V)\Lambda_0 : (\ \varepsilon_{tot} - \varepsilon_{th} - \varepsilon_{tr} - \varepsilon_{cr}) \tag{6.38}$$

Now the mechanical equilibrium equation that gives the *Linear momentum conservation equation of a multi-phase medium*, [D.Gawin et al., 2005] is shown bellow:

$$div(\sigma'' - \alpha p^s I) + \rho g = 0 \tag{6.39}$$

A total effect of the mechanical and thermo-chemical damages is defined by the total damage parameter:

$$D = 1 - (1 - d) \cdot (1 - V) \tag{6.40}$$

The simplifications made also influence the stress state. An elastic stress/strain relation will be used and the stresses will be computed as in equation 6.41 where E is Young's modulus.

$$\sigma = E \cdot \varepsilon_{total} \tag{6.41}$$

6.4 Overview

This chapter contains the mathematical model for the transport equations of heat and mass as well as mechanical aspects as strain and stresses. Because of lack of experimental data some simplifications had to be adopted in a way suitable for keeping the physical meaning of the phenomena.

The governing equations presented above can be solved using different analytical or numerical methods. In the next chapter, a numerical model for solving these equations will be presented.

Chapter 7

Numerical Model of The Transport Process

This chapter starts with a brief description of the finite element method. After this an illustration of the geometry and discretization over space of the concrete member is made. A first steady state problem followed by a transient one are presented along with boundary and initial conditions. The transient problem is discretized by an implicit difference scheme and then solved using the Newton Raphson method. In the end, an overview about the chapter will be made.

7.1 Finite element method

As stated in the previous chapters, a global model that encounteres for all the factors influencing the spalling phenomenon and changes in concrete during fire cannot be implemented yet. Even so, parameters that have bigger impact for spalling to occur can be modeled numerically, by using several approaches within also the finite element method.

The finite element method is a numerical approach by which general differential equations can be solved in an approximate manner, [N.Ottosen and H.Peterson, 1992]. In this case, a one dimensional model is chosen as a region over which the differential equations define the physical problem. The main feature of this method is the division of the entire region into smaller parts, finite elements, and the principle is that if the equations hold for the whole region, they will also approximate the phenomenon over each element. Therefore the parameters influencing spalling will be modeled based on the above mentioned idea.

7.2 Geometry

Figure 7.1 presents the real geometry of a tunnel exposed to fire, considering that fire starts at the bottom part and that propagates inside the tunnel room throughout convection (from the surrounding air) or radiation (direct flame contact), both convective and radiation heat fluxes inducing an increase of the element temperature.
Fire in a tunnel is a complex phenomenon and lots of parameters such as ventilation control, stratification of smoke, geometrical characteristics(tunnel slope, cross sectional area, length) etc. need to be considered when modelling fires effect in a tunnel. But because the interest in this thesis is only the fire behavior of concrete as a material, in the

finite element approach this geometry is simplified and the factors earlier mentioned are not taken into account.

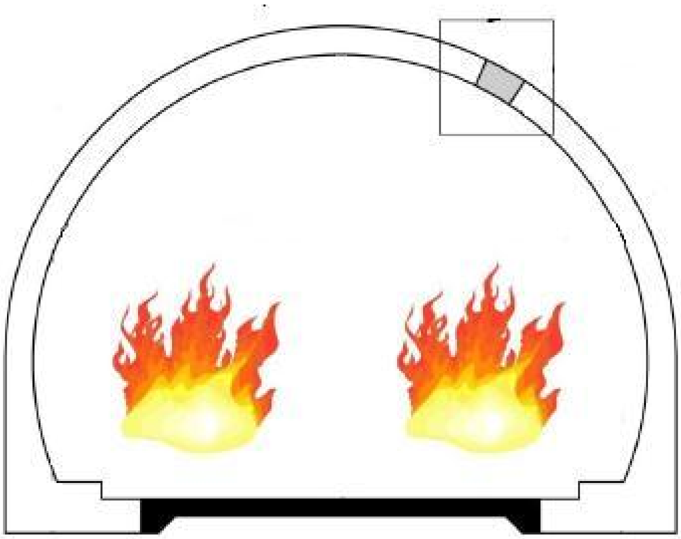

Figure 7.1. Real model

From the whole tunnel only a part is taken into account, the square on the top part, where a grey side was depicted. This simplification can be done because of the same comportment of the involved factors, no matter the position.

Another simplification regards the heat transfer. The transmission of the heat within the member takes place through *conduction*, a mechanism specific for solid materials that is done via the contact between atoms and molecules in the substance involving also transfer of kinetic molecular energy.

On the outside surface, the first node will be subjected to convection and radiation by the surrounding medium and the last one to ambient conditions. This will be done by the imposed boundary conditions. In this way focus will be given only on what happens inside the element.

The finite element formulation of this section can be seen in figure 7.2. This discretization over space contains the nodes, the unknowns numbering that are the degrees of freedom (dof), represented by the temperature, moisture content (in terms of capillary pressure) or vapor pressure in each node, also element numbering and topology (which nodes define the element), [Clausen, 2009].

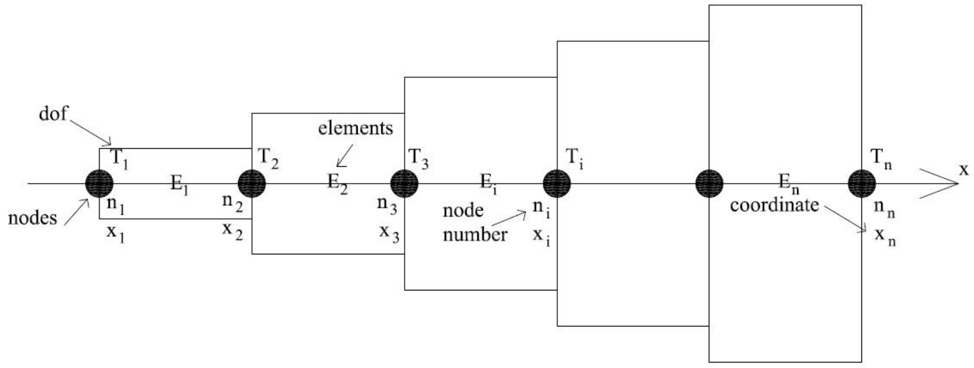

Figure 7.2. Element discretization, inspired from [Clausen, 2009]

The geometry and discretization over space represents a common point for temperature, moisture content or vapor pressure. Their distribution inside the concrete member is obtained by using same numerical equations, but the terms concerning each parameter are different. The next table sets a correlation between the factors. All the coefficients from table 7.2 were defined in the previous chapter, *Mathematical model.* From now on, global parameters that will be used will be X, ψ, κ and J.

	X	ψ	κ	J
Heat transfer	T	ρc	k	q
Moisture diffusion	p^c	$\eta^g \rho^{gw}$	$\rho^v \frac{kk_{ra}}{\mu_g}$	J_v
Gas diffusion	p^g	$\eta^g \rho^{ga}$	$\rho^a \frac{kk_a}{\mu_{ga}}$	J_{ga}

7.3 Steady state distribution

In the very beginning a steady state distribution independent of time was considered. Making a correlation with the *Mathematical model*, this state is modeled using the equations from the heat and mass transfer equations. It can be indicated that the partial differential equations from chapter 6 represents the strong formulation and the weak formulation is presented in this chapter.
The parameters do not depend on temperature/moisture content, therefore the problem is a linear one and it can be solved following [D.Cook et al., 2002]:

$$\begin{bmatrix} \frac{\kappa}{L} & -\frac{\kappa}{L} \\ \frac{\kappa}{L} & \frac{\kappa}{L} \end{bmatrix} \begin{Bmatrix} X_1 \\ X_2 \end{Bmatrix} = \begin{Bmatrix} J_1 \\ J_2 \end{Bmatrix} \tag{7.1}$$

The first matrix represents the element conductivity matrix, known as the stiffness matrix in structural dynamics. All this formulation is valid for one single element E_i of length L within the whole region. For it to be applicable to the entire region, a global conductivity matrix $[K]$ needs to be formed.

An example of how the global conductivity matrix is computed is shown below for 2 elements with 3 nodes. The same principle is applied for more elements. In this case, it is considered that all elements have the same material properties.

$$[K] = \begin{bmatrix} \frac{A\kappa}{L} & -\frac{A\kappa}{L} & 0 \\ -\frac{A\kappa}{L} & \frac{A\kappa}{L} + \frac{A\kappa}{L} & -\frac{A\kappa}{L} \\ 0 & -\frac{A\kappa}{L} & \frac{A\kappa}{L} \end{bmatrix} \tag{7.2}$$

Two boundary conditions were implied for each case. It was supposed that the temperature at the cold side is T_{cold}=20°C, respectively the relative humidity $RH = 0.6\%$. At the hot surface, the temperature was considered T_{hot}=1000°C and $RH = 0\%$.The vapor pressure was considered as being equal with the atmosphere pressure $P = 101325Pa$ at both sides.

After introducing the boundary conditions and assembling the global matrix, the final global system of equation can be solved:

$$\begin{bmatrix} K_{11} & K_{12} & ... & K_{1n} \\ K_{21} & K_{22} & ... & K_{2n} \\ ... & & & \\ K_{n1} & K_{n2} & ... & K_{nn} \end{bmatrix} \begin{Bmatrix} a \\ X_2 \\ ... \\ X_n \end{Bmatrix} = \begin{Bmatrix} J_1 \\ b \\ ... \\ J_n \end{Bmatrix} \tag{7.3}$$

Then, the defined X are multiplied with their respective columns of K and transferred to the right-hand side:

$$\begin{bmatrix} K_{22} & K_{23} & ... & K_{2n-1} \\ K_{32} & K_{33} & ... & K_{3n-1} \\ ... & & & \\ K_{n-12} & K_{n-13} & ... & K_{n-1n-1} \end{bmatrix} \begin{Bmatrix} X_2 \\ X_3 \\ ... \\ X_{n-1} \end{Bmatrix} = \begin{Bmatrix} b \\ c \\ ... \\ n-1 \end{Bmatrix} - a \begin{Bmatrix} K_{21} \\ K_{31} \\ ... \\ K_{n1} \end{Bmatrix} - n \begin{Bmatrix} K_{1n} \\ K_2n \\ ... \\ K_{n-1n} \end{Bmatrix} \tag{7.4}$$

Finally, the unknowns can be found from the reduced K matrix and applied boundary conditions. This case was considered for a starting point, in order to have an idea of how to model more complicated problems, when also time is involved.

7.4 Transient state

In reality, the problem is more complex and the involved coefficients change in time with the temperature increase, as presented in chapter 4.

For a transient analysis the equation that needs to be solved are the balance (conservation) equations presented in the chapter *Mathematical model*. For example, for the temperature distribution the *Enthalpy balance equation of a multi-phase medium* is transformed accordingly to the finite element method. For making it easier to visualize the correlation between the two, the mathematical expression will be shown again.

$$(\rho C_p)_{eff}\frac{\partial T}{\partial t} - div(\chi_{eff} gradT) = -\dot{m}_{vap}\Delta H_{vap} + \dot{m}_{dehydr}\Delta H_{dehydr} \tag{7.5}$$

The finite element equation is, D.Cook et al. [2002]:

$$[C]\{\dot{T}\} + [K_T]\{T\} = \{R_T\} \tag{7.6}$$

Where:

$[R_T]$	Thermal load vector [W]
$[C]$	thermal capacity matrix[J/kgK]
$[K_T]$	conductivity matrix[W/mK]

Making an association with the mathematical model, the first term represents the rate at which the heat is stored in the material. Therefore the second term in equation 7.6 represents the internal heat transfer and the part from the right-hand side depends on the hydration-dehydration and evaporation processes and on the fire boundary conditions. Same principle is applied for the other equations, with the difference that $[R_T]$ will be the hygral load vector(contains also the boundary conditions), [C] can be seen as a general capacity matrix and [K] as a general conductivity matrix.

The conductivity matrix $[K_T]$ may be associated with the stiffness matrix, as before and the capacity one $[C]$ with the mass matrix from structural dynamics. This way it is easier to define the $[C]$ matrix, following the same principle as for the mass matrix. Therefore, $[C]$ will be represented as a lumped matrix. This means that it will be a diagonal matrix and according to [D.Cook et al., 2002] the lumped matrix has the advance of being computational, less storage space and processing time required than for the consistent matrix.

First, the capacity matrix was computed for one finite element with two nodes, where in each node a lumping particle of $(\psi dL)/2$ was placed. As a result the capacity matrix for one element has the following form:

$$[C] = \frac{\psi dL}{2}\begin{bmatrix} 1 & 0 \\ 0 & 1 \end{bmatrix} \tag{7.7}$$

Because now the parameters change, the matrixes will be assembled using the same principle as before, but with different input parameters for every node. An example for the [K] matrix is provided below.

$$[K] = \begin{bmatrix} \frac{A\kappa_1}{L} & -\frac{A\kappa_1}{L} & 0 \\ -\frac{A\kappa_1}{L} & \frac{A\kappa_1}{L} + \frac{A\kappa_2}{L} & -\frac{A\kappa_2}{L} \\ 0 & -\frac{A\kappa_2}{L} & \frac{A\kappa_3}{L} \end{bmatrix} \tag{7.8}$$

The load vector R_T contains in the first and last node the imposed boundary conditions (BC), that will be explained later and in between $-\dot{m_{vap}}\Delta H_{vap} + \dot{m_{dehydr}}\Delta H_{dehydr}$, that change according to the temperature and refer to the exotermic reactions that happen inside the element. For computing the moisture content, this vector will contain between the mass source term related to evaporation process and the on related to hydration-dehydration.

$$R_T = \left\{ \begin{array}{c} BC \\ -m_{\dot{v}ap}\Delta H_{vap} + m_{deh\dot{y}dr}\Delta H_{dehydr} \\ \dots \\ BC \end{array} \right\} \tag{7.9}$$

7.4.1 Boundary and initial conditions

There are several ways of expression boundary conditions, *Dirichlet boundary conditions*, *Newmann condition* and *convective surface condition*, [Majumdar, 2005]. In this case, boundary conditions of the first kind will be used. For example the surface temperature is specified as function of space and time and not as a heat flux.

The bondary conditions are imposed in a way to try to simulate the real fire scenario. They will regard side (I) and (II) from figure 7.3.

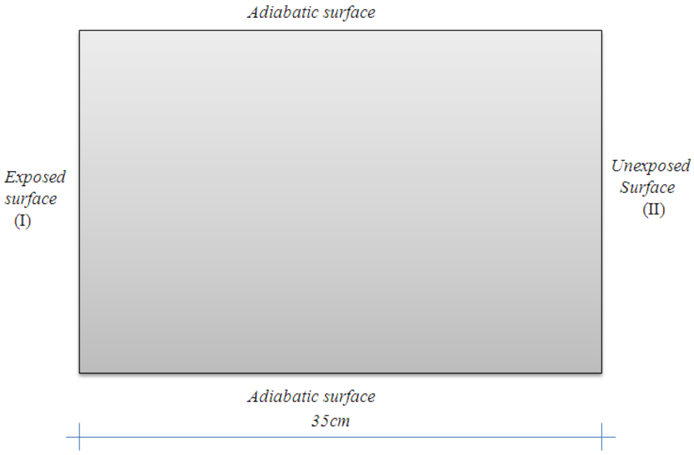

Figure 7.3. Boundary condition for the concrete element

For side (I) the transient heating is done following the standard temperature-time ISO-834 curve that has the expression given by equation 7.10, where t represents the time in minutes.

$$T_{ISO} = 345log(8t+1) + 293.15 \tag{7.10}$$

A seen from the mathematical formulation and figure 7.4 this fire simulates a rather "intense" fire, being representative for a rapid heating and for a severe fire case.

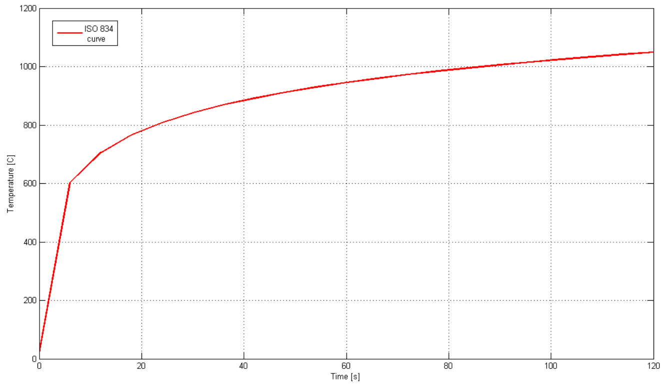

Figure 7.4. The ISO 834 fire curve

Regarding the vapor dissipated into the surroudings, the water capillary pressure is $p^c = 800MPa$ and the gas pressure is equal to the atmospheric pressure $p^g = 101325Pa$.

On the unexposed side (II), ambient conditions are imposed and that are a temperature of $T = 20°\text{C}$.

As initial conditions, for time $t = 0$:

- The temperature is equal to $T = 20°\text{C}$
- Relative humidity RH=60%
- Gas pressure $p^g = 101325\text{Pa}$

7.4.2 Numerical solution

Having defined all the needed parameters, equation 7.6 can be solved numerically. Because the involved parameters depend on the changes in time, the actual equation to be solved is:

$$[C(X)]\{\dot{X}\} + [K_T]\{X\} = \{R_T(X)\} \tag{7.11}$$

Knowing that two unknowns $\{X\}_n$ and $\{X\}_{n+1}$ are parted by a time step Δ_t, the time dicretization can be done by a difference scheme, [D.Cook et al., 2002]:

$$\begin{aligned} (\frac{1}{\Delta_t}[C(X_{n+1})] + \beta[K_T(X_{n+1})])\{X\}_{n+1} = \\ (\frac{1}{\Delta_t}[C(X_{n+1})] - (1-\beta)[K_T(X_{n+1})])\{X\}_n + (1-\beta)\{R_T\}_n + \{R_T\}_{n+1} \end{aligned} \tag{7.12}$$

As seen there is a coefficient β that is related to the accuracy and stability of the algorithm. The value of β is set to 1, meaning that the algorithm is unconditionally stable,[D.Cook et al., 2002]. Therefore β equal to 1 provides some simplifications:

$$(\frac{1}{\Delta_t}[C(X_{n+1})] + [K_T(X_{n+1})])\{X\}_{n+1} = \frac{1}{\Delta_t}[C(X_{n+1})]\{X\}_n + \{R_T\}_{n+1} \tag{7.13}$$

This new equation was solved using two approaches for computing the temperature. Only the first approach was used for computing the moisture content and the gas pressure. For the temperature both approaches were implemented.

In the first case, a simpler way was used. The temperature was computed considering that the specific heat changes with temperature following the trend presented in the [EC2-EN1992-1-2, 2005] and presented in chapter 6. The conductivity k was taken as a constant. Also density of water vapor and density of dry air were taken as constants. The temperature distribution will further influence the relative humidity and vapor pressure.

From equation 6.1.1 in chapter 6 it can be noticed that the change of the speciffc heat is rather smooth, after 400° the value is constant, therefore equation 7.13 can be solved in a simpler manner using just the time discretization and initial conditions.

In the second approach, all parameters involved in the calculation were considered to change at every iteration and also every time step.
Therefore, equation 7.13 will be solved using the *Newton- Raphson method.* The *Newton-Raphson method* is an iterative procedure for time independent nonlinear problems where the solution at the first time step is given and the result of the equation is known for every time step. The unknown is computed with the help of a tangent matrix updated at every time step.

First the whole expression will be denoted as $F(X_{n+1})^{k+1}$, where k represents the iteration index. Therefore:

$$F(X_{n+1})^{k+1} = [C(X_{n+1})]\frac{\{X\}_{n+1} - \{X\}_n}{\Delta_t} + [K_T(X_{n+1})])\{X\}_{n+1} + \{R_T\}_{n+1} \tag{7.14}$$

$$F(X_{n+1})^{k+1} = 0 \tag{7.15}$$

The solution of F has the expression from 7.16, where J represents the tangent matrix.

$$X_{n+1}^{k+1} = X_{n+1}^{k} - J^{-1}(X_{n+1}^{k})F(X_{n+1}^{k}) \tag{7.16}$$

The tangent matrix is updated at every time iteration:

$$J = K_T + \frac{\partial K_T}{\partial T} \cdot K + (\frac{\partial C}{\partial T} + C) \cdot \frac{1}{\Delta_t} \tag{7.17}$$

As a starting point, $\{X_0\}$ will be given, for example the temperature at t=0, $\{T_0\} = 20°\text{C}$. The second value will be approximated using the following expression. To be noticed that at the first step the tangent matrix is equal to the K matrix at time t=0.

$$\{X_1\} = X_0 - J^{-1}(F(X_0)) \tag{7.18}$$

Knowing the first two values, a more accurate solution was found for the following ones, within an iteration proces. The results will be exposed in the separate chapter.

The before presented numerical solution was used to computed the temperature distribution, capillary pressure and gas pressure. Having this distribution other parameters were found analytically, as for example the relative humidity RH, the degree of saturation with liquid water, etc. based on the equations presented in chapter 6.

7.5 Overview

The finite element method provides a strong and simplified tool (compared to the analytical of finite difference- control volume) for modeling the distribution of the temperature, moisture content and gas pressure inside a concrete element. The computation can be simple or complicated depending on the available input parameters (for the temperature distribution all the parameters were taken as variable, but for the water model due to lack of data some of the input parameters were taken as constants from experimental works). A strong correlation between the mathematical model and the finite element model can be seen.

Chapter **8**

Numerical Model of the Stress State

This chapter will start with a description of the "Initial strain method" used for computing the thermal and the shrinkage strains and stresses. Parameters involved in this method will be explained. The new mesh of the member will be presented along with the changes involved by using isoparametric quadrilateral four noded elements. In the end a brief summary is carried out.

In the *Mathematical model* chapter several types of strains were explained and their sum up forms the final total strain. Unfortunately, due to lack of experimental data, only the thermal and the shrinkage strain can be computed numerically and the total strain will be approximated based on these values. The method will be explained in detail for the thermal stresses. The principle is the same for the shrinkage stresses, the only difference being the shrinkage coefficient instead of the thermal dilatation one and the water content instead of temperature.

The numerical code for modeling this parameters is done in such a way that, if desired, elastic strains (from mechanical loads) can also be taken into account and added to the final strain.

8.1 "Initial strain method"

The calculations are based on the *Initial strain method*, [R.W.Lewis, 1996]. This implies computing the initial strains and stresses produced by the temperature field when all displacement are prohibited. These stresses are converted to equivalent nodal forces that are applied to the system and then the strains and stresses produced by this force can be computed from the displacement obtained. The final real stresses and strains are calculated by superposing the obtained values with the initial stresses calculated in the begining, [D.Cook et al., 2002].

As a first step, the initial thermal strain for one element is defined as in equation 8.1. As seen from the definition a *plane strain* situation is taken into account, highlighted by the presence of the Poisson ratio, ν. In plane strain the body is kept still in the z direction, but as it will start to be heated it will try to expand in all three directions. It cannot resulting in an exial expansion that tries to "overflow" in the lateral dimensions (Poisson ratio effect).

$$\epsilon_0 = (1+\nu)\begin{bmatrix} \epsilon_{x0} \\ \epsilon_{y0} \\ \gamma_{xy} \end{bmatrix} \tag{8.1}$$

Normally Poisson ratio changes its value with increasing temperature, experimental work confirming a reduction of Poisson's ratio, [Kassir et al., 1996]. Other experiments were conducted by [J.C.Marechal, 1972], and approve the reduction of Poisson's ratio, but in both cases the measurements do not exceed 400°C. The reasons for decrease are the weakening of the microstructure because of rupture of bonds at heating, effects of transient moisture state and drying, [Bažant and Kaplan, 1996] and cracking.

Because of lack of data and need of further research in this matter, Poisson's ratio will be taken as a constant of 0.3. Strains will be developed in the x and y direction (in plane strain $\epsilon_z = 0$) and the shear strain will be 0.

The initial strain has the final expression as in equation 8.2. The α_1 and α_2 coefficients represent the thermal dilatation in the x, respectively y direction that are determined experimentally and are temperature depedent. In the present model they were taken as equal, α_1=α_2 assuming that the thermal dilatation is the same in both directions.
In the case of the shrinkage strain, α was taken as a constant value of 10^{-5}, [Bažant and Kaplan, 1996]. Because the temperature is not constant along the length of the member, ΔT was calculated as an average temperature between two nodes (from the numerical model of the temperature distribution). To be noticed that ΔT in a point is independent of direction, having a common value for both x and y.

$$\epsilon_0 = (1+\nu)\begin{bmatrix} \alpha_1\Delta T \\ \alpha_2\Delta T \\ 0 \end{bmatrix} \tag{8.2}$$

The actual "transformation" of the temperature rise ΔT into a mechanical force is done through equation 8.3. This forces will try to stretch the element in the same way as a mechanical force will do. As seen, the force expression takes into account the geometrical perspective through B^T and the material one through matrix D.

$$F_0 = \int_A B^{\mathrm{T}} D \epsilon_0 \; t \; dA \tag{8.3}$$

Matrix D is called the constitutive matrix and as stated before takes into account material parameters. It can be different depending on situation, plane strain or plane stress. As the present situation is a plane strain, D has the expression:

$$D = \frac{E}{(1+\nu)\,(1-2\,\nu)} \begin{bmatrix} 1-\nu & \nu & 0 \\ \nu & 1-\nu & 0 \\ 0 & 0 & \frac{1}{2}\,(1-2\,\nu) \end{bmatrix} \tag{8.4}$$

In an attempt to follow the real development as closely as possible, the Young's modulus E was decreased as temperature increased using the trend seen in figure 8.1. The relative modulus of elasticity represents the ratio between the temperature dependent Young's modulus $E(T)$ and the undamaged E at ambient conditions.

$$\text{Relative modulus of elasticity} = \frac{E(T)}{E_{20^\circ C}} \tag{8.5}$$

Until the temperature reaches 150° Young's modulus remains at its initial value, the ratio being equal to 1, and then it starts decreasing. Physically it is impossible that E reaches 0, therefore a minor alteration that retards the decrease of E is represented by the dotted line, [Buchanan, 2001].

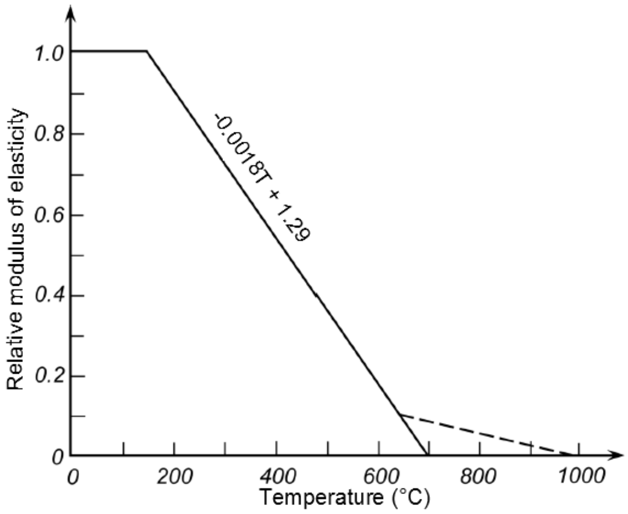

Figure 8.1. Young's modulus decrease with temperature increase, [Buchanan, 2001]

Having the force that is applied to the system, equation 8.6 is solved. K is known and it represents the stiffness matrix that will be explained in the following section along with the before mentioned B matrix. From here the displacement vector U will be computed. Vector F can be the F_0 vector plus some mechanical forces or just F_0. If mechanical load are applied they will be superposed on the thermal loads and the final force vector will be assembled in a similar way as the stiffness matrix.

$$K \cdot U = F \tag{8.6}$$

Now the real stresses and strains can be found. The strains are found directly from the displacement vector and then the stresses are superposed with the initial strain.

$$\epsilon = B \cdot U \tag{8.7}$$

$$\sigma = D \cdot (\epsilon - \epsilon_0) \tag{8.8}$$

8.1.1 Transient regim

As the problem treated is a transient one, a suitable numerical algorithm was adopted. The steps presented bellow were implemented in the numerical code. The main principle is based on a big loop regarding the time increment within which the second loop over the entire domain is generated. The node and element numbers are the same as before in order to match the temperature distribution. The first three steps are outside the loops and steps a,b,c and d are contained in the domain loop.

1. Load the temperature(relative humidity) distribution calculated before at each time step $t + n\Delta t$
2. Compute the change in temperature δT for every time step as the average temperature between two nodes
3. Compute E for every time step according to the temperature
4. For a single time step t (time loop):
    a) Computed D, K and $F_0(\epsilon_0$ is included here) for every element
    b) Assemble K and F for the whole member
    c) Solve $K \cdot U = F$
    d) From U find the real strains and stresses
5. Go on to the next time step t + Δt starting from point 4

Regarding boundary conditions, it is assumed that the concrete element can deform freely in the side exposed to fire and it is constrained on the other side (see figure 8.2). The forces are applied as tension forces for the thermal stress analysis and as compression forces for the shrinkage stresses.

8.2 Definition of the geometry and stiffness matrix

The stress distribution represents a two dimensional problem, therefore a new geometry for the elements was adopted using isoparametric quadrilateral four noded elements(IsoQ4).

The mesh of the member can be seen in figure 8.2. In the actual calculations more elements were used, but because of clearity reasons the plot contains only 10 elements. Keeping the same conditions as before, the left side, starting from element 1, will be the exposed to fire conditions and the right side is the one that fullfils normal conditions.

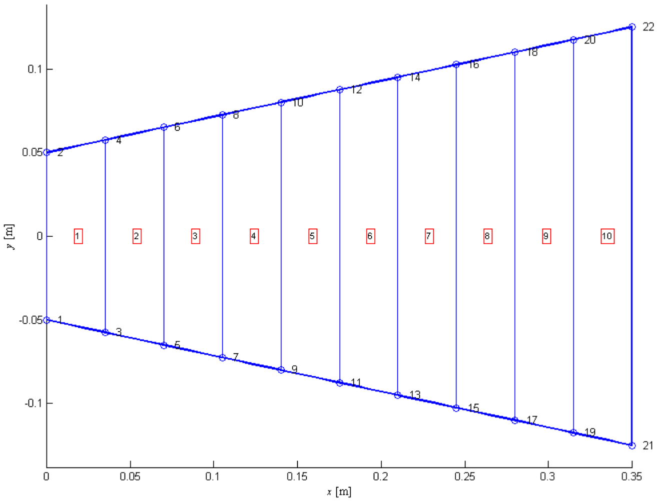

Figure 8.2. Model geometry

As mentioned the new elements used are no longer linear ones as before but isoparametric quadrilateral four noded elements. The IsoQ4 element is a rectangle that has linear shape functions, as seen later on in equation 8.9, meaning that it can only have straight sides but it is not able to bend its shape. An example of IsoQ4 element is illustrated in figure 8.3.

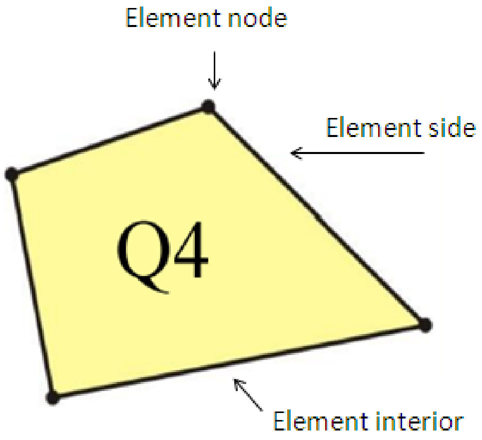

Figure 8.3. Isoparametric four-noded quadrilateral element, [Clausen, 2009]

The IsoQ4 elements use an auxiliary coordinate system symbolized by the ξ and

η axes. The role of this new coordinates is to transform a given element into a reference element that is a square, as seen in figure 8.4. The location of the physical element is called the *Global domain* and the quadratic area, where it is also easier to perform the calculations, is called *Parent domain.* A point in the real element can then be referred to by the coordinates in the parent domain.

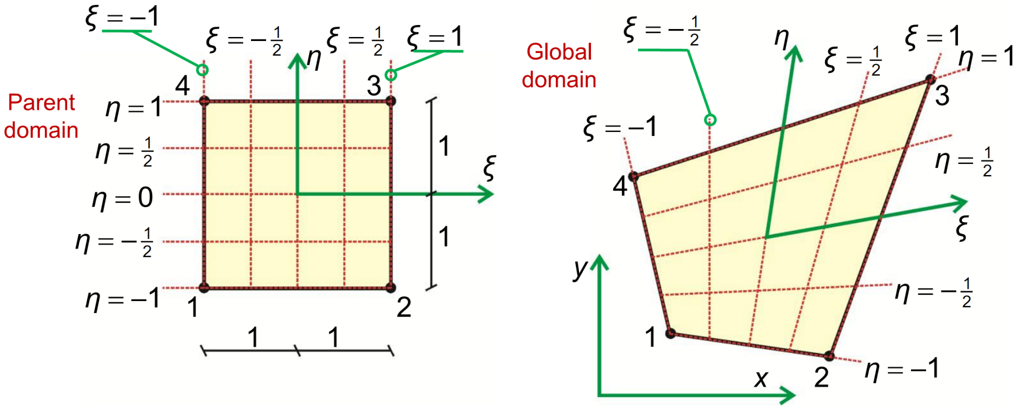

Figure 8.4. Parent and global domain of IsoQ4 elements, [Clausen, 2009]

The mapping of elements is done with the help of the shape functions. The interpolation between the nodes and the IsoQ4 linear shape functions can be seen bellow:

$$
\begin{aligned}
x &= \sum_{i=1}^{n_{node}} N_i(\xi,\eta)x_i \\
y &= \sum_{i=1}^{n_{node}} N_i(\xi,\eta)y_i \\
N_1 &= \tfrac{1}{4}\ (1-\xi)\,(1-\eta) \\
N_2 &= \tfrac{1}{4}\ (1+\xi)\,(1-\eta) \\
N_3 &= \tfrac{1}{4}\ (1+\xi)\,(1+\eta) \\
N_4 &= \tfrac{1}{4}\ (1-\xi)\,(1+\eta)
\end{aligned}
\tag{8.9}
$$

Having defined the shape functions, the matrixes presented in the previous section can be defined. The first one was matrix B that takes into account the geometry of the element. Because the shape functions are defined in the parent domain, and the derivative matrix B should be in global domain, three new matrices are introduced: $B = H \cdot J_{exp}^{-1} \cdot D_{N,exp}$. The matrix H then relates the derivatives with the actual strain in the element:

$$
H = \begin{bmatrix} 1 & 0 & 0 & 0 \\ 0 & 0 & 0 & 1 \\ 0 & 1 & 1 & 0 \end{bmatrix}
$$

The matrix $D_{N,exp}$ relates the nodal displacements U with the derivatives in parent domain. $D_{N,exp}$ is an expanded form of the D_N matrix:

$$D_{\mathrm{N}} = \begin{bmatrix} \frac{\delta N_1}{\delta \xi} & \frac{\delta N_2}{\delta \xi} & \frac{\delta N_3}{\delta \xi} & \frac{\delta N_4}{\delta \xi} \\ \frac{\delta N_1}{\delta \eta} & \frac{\delta N_2}{\delta \eta} & \frac{\delta N_3}{\delta \eta} & \frac{\delta N_4}{\delta \eta} \end{bmatrix}$$

$$D_{\mathrm{N,exp}} = \begin{bmatrix} D_{\mathrm{N},11} & 0 & D_{\mathrm{N},12} & 0 & D_{\mathrm{N},13} & 0 & D_{\mathrm{N},14} & 0 \\ D_{\mathrm{N},21} & 0 & D_{\mathrm{N},22} & 0 & D_{\mathrm{N},23} & 0 & D_{\mathrm{N},24} & 0 \\ 0 & D_{\mathrm{N},11} & 0 & D_{\mathrm{N},12} & 0 & D_{\mathrm{N},13} & 0 & D_{\mathrm{N},14} \\ 0 & D_{\mathrm{N},21} & 0 & D_{\mathrm{N},22} & 0 & D_{\mathrm{N},23} & 0 & D_{\mathrm{N},24} \end{bmatrix} \tag{8.10}$$

The inverse Jacobian matrix J_{exp}^{-1} then translates the derivatives in parent domain coordinates to global domain coordinates, x and y.

$$J = \begin{bmatrix} \sum_{i=1}^{n_{node}} \frac{\partial N_i}{\partial \xi} x_i & \sum_{i=1}^{n_{node}} \frac{\partial N_i}{\partial \xi} y_i \\ \sum_{i=1}^{n_{node}} \frac{\partial N_i}{\partial \eta} x_i & \sum_{i=1}^{n_{node}} \frac{\partial N_i}{\partial \eta} y_i \end{bmatrix}$$

$$J_{\mathrm{exp}}^{-1} = \begin{bmatrix} J_{11}^{-1} & -J_{12}^{-1} & 0 & 0 \\ -J_{21}^{-1} & J_{22}^{-1} & 0 & 0 \\ 0 & 0 & J_{11}^{-1} & -J_{12}^{-1} \\ 0 & 0 & -J_{21}^{-1} & J_{22}^{-1} \end{bmatrix} \tag{8.11}$$

Now the stiffnes matrix of an isoparametric quadrilateral element can be defined:

$$K = \int_{-1}^{1} \int_{-1}^{1} (H \cdot J_{exp}^{-1} \cdot D_{N,exp})^T t D (H \cdot J_{exp}^{-1} \cdot D_{N,exp}) det(J) d\xi d\eta \tag{8.12}$$

This represents an integration over a matrix of non-linear functions and therefore a numerical integration will be used to integrate over the area of the element in the parent domain, by using Gauss quadrature.
The integration is performed by evaluating the integral in the Gauss points and summing each value by a weight factor W. With a Gauss order of n = 2, the locations of the points and weight factor are $\xi = \eta = \pm\frac{1}{\sqrt{3}}$ and W=1.

8.3 Sum up

A solution of thermal/shrinkage stress development was adopted connecting heat transfer analysis with stress analysis. This solution can extend also to different elements, that will require changes of the element geometry (shape functions). The time-varying stresses pattern is achieved by stepping forward in time, using the transient temperature analysis. Other strains, like the thermo-chemical strain increment cannot be computed using the *Initial strain method* because the mathematical modeling of the chemical shrinkage coefficient depents on several complicated endothermic reactions, [Gawin et al., 2002]. Even so, with the simplification involved, the numerical model for the strains and stresses follows a close to reality example.

Chapter 9

Results

Results from the finite element method will be exposed concerning plots with temperature distribution, moisture content and gas pressure along with adjacent plots that are connected to these factors. Thermal and shrinkage strains will be illustrated and then the effective stresses will be exposed. Interpretations of the obtained outcomes will be given and a short sum up will be provided.

9.1 Review

A brief review of the analyzed model will be sketched using figure 9.4. As seen, the wall has a 35cm thickness, exposed to the ISO 834 fire on one side and to ambient conditions to the other side. The total time of fire exposure was considered approximately 27min. The height of the model is not relevant as the model is a 1D model and only the transport along x-axis is of interest. The results will investigate what happens inside the element due to fire exposure.

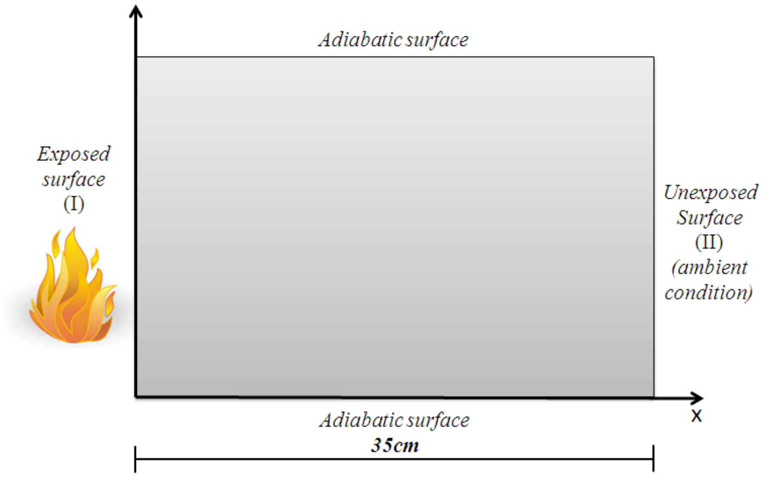

Figure 9.1. Concrete element exposed to fire

9.2 Distribution of fields of interest

As presented in the previous chapter, the calculation started from a simple case, the steady state, in order to have a general idea of the concrete behavior in fire, going further into transient state with factors depending on the temperature increase, in a way to get closer to the real case of a fire scenario. Because the main interest is on the transient state, the steady state results will be exposed and only brief explanations will be given.

The temperature in steady state can be seen in figure 9.2. In this simple case, the thermal conductivity was taken as constant and boundary conditions like 900°C on the hot face and 20°C on the cold face were imposed.

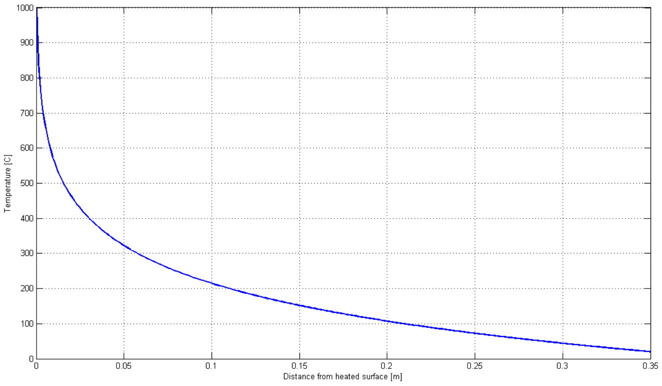

Figure 9.2. Temperature distribution along the element

The capillary pressure was computed in order to find the relative humidity that is a characteristic parameter for defining the moisture inside the concrete.

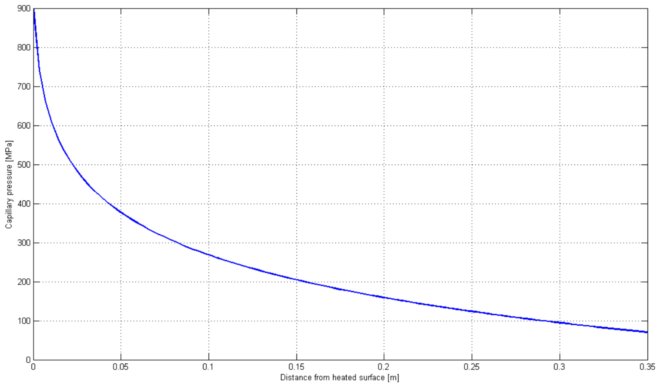

Figure 9.3. Capillary pressure along the element

The RH was computed analytically from the capillary pressure distribution. Near the surface, the RH is equal to 0, than is has a peak, symbolizing the saturation with liquid and vapor, the region known as moisture clog. After this is starts decreasing and reaches its initial value set in the boundary conditions.

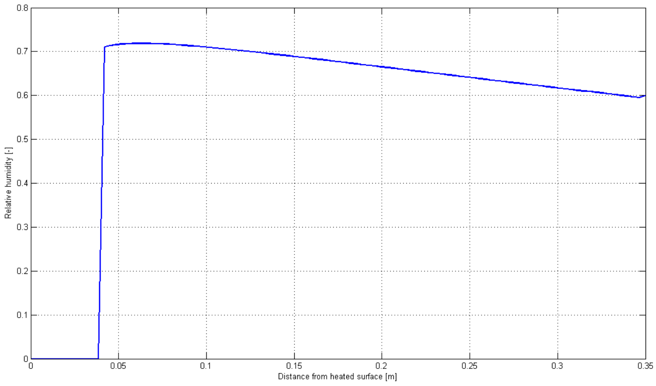

Figure 9.4. Relative humidity along the element

The gas pressure is illustrated in figure 9.5. It can be noticed that its peak coincides with the position of the saturation front.

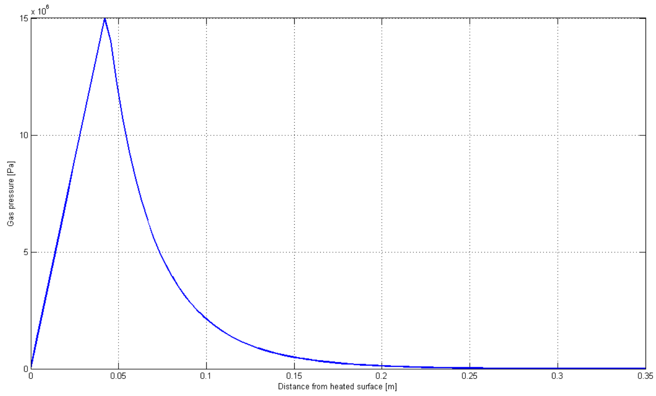

Figure 9.5. Gas pressure along the element

The main field of interest regards the temperature, relative humidity and gas pressure distribution in a transient regim. Then other fields connected to these ones will be plotted and explained.

9.2.1 Temperature distribution

The transient temperature distribution can be seen in figures 9.6 and 9.7. As a general remark it can be seen that the trend of both figures follows the same path. At the exposed side the temperature increases fast, according to the imposed boundary conditions (Iso834 fire) and then decreases until it reaches 20°C at the cold side. From the hot site it can be seen that the heating rate is quite fast. In the first 3 minutes the surface reaches a high temperature of approximately 600°C. The fast increase continues and after 10 minutes a temperature of 700°C is reached. After this, the increase continues, but is less rapid and finaly at 27 minutes reaches a value of 850°C.

Due to low conductivity of concrete, $k = 1.6 W/m°C$, the temperature drops from a real high value to a small one, in a relative short distance, $35cm$. It is important to see that the major drop takes place in the first 5 cm of material.

This is an example of the good fire behavior of concrete, the temperature decreases in a relatively short distance from the heated surface. As it is considered that concrete is not damaged until it reaches 500°C, [EC2-EN1992-1-2, 2005], from this point of view it can be stated that the damage is rather minor in this case, temperatures above 500°C are only very close to the surface, less than 2cm inside the core.

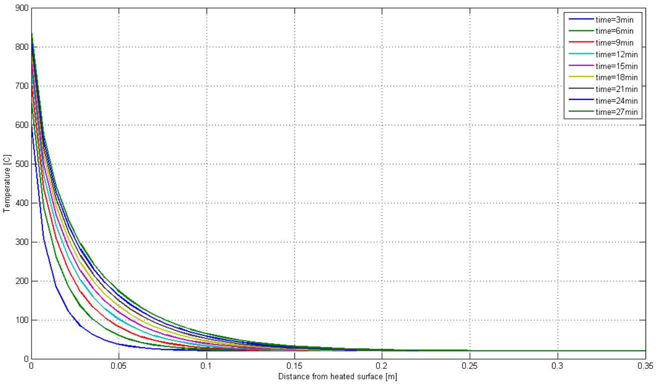

Figure 9.6. Temperature distribution using constant parameters

Regarding the difference between the two figures, it can be seen that the variation of the parameters has not such a big influence on the results. The curves are more connected in the model that uses variable parameters, meanwhile the distance between them increased when using constant variables.
As the distance between the curves has to do with the accumulation of internal energy, it can be said that for the first case less energy is stored inside than for the second case. Also the numerical method of computing was different and might influence the trend.

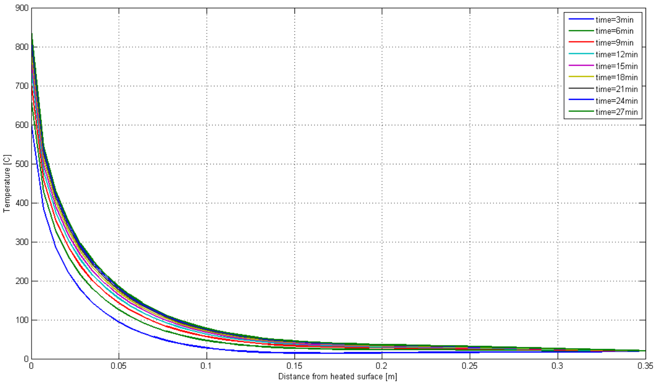

Figure 9.7. Temperature distribution using temperature dependent parameters

9.2.1.1 Moisture distribution

As presented in chapter 6 *Mathematical model*, the moisture content is composed of liquid water and water vapor. The diffusion of moisture driven by the gradient of moisture concentration is assumed negligible in view of the fact that the diffusion takes time [Bažant and Kaplan, 1996] and fire spalling occurs quite fast, in the first minutes of heating. Therefore, the moisture distribution was modeled using a gradient of capillary pressure. The distribution of capillary pressure can be seen in figure 9.8. This plot is valid only for values of temperature lower than the critical temperature value of 375°. After this point there is no more capillary pressure.

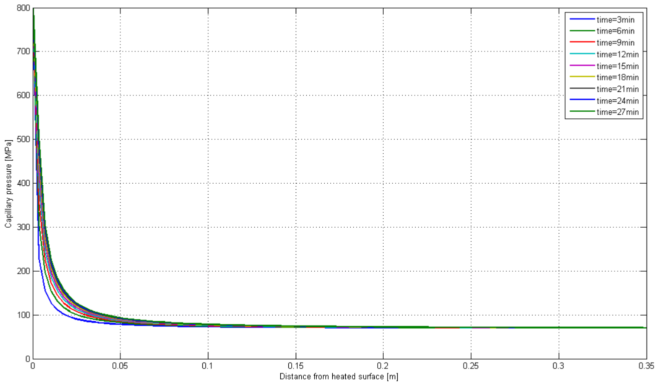

Figure 9.8. Capillary pressure distribution

Knowing the capillary pressure, the moisture distribution was computed in terms of relative humidity, RH. The results are presented in figure 9.9. It can be seen that in the begining the relative humidity is close to its initial value and then while time passes and temperature increases at the exposed side, RH moves inside the element core where, when meeting lower temperatures it goes back to its initial value. This plot also illustrates the fact that part of the moisture goes out and part is driven inside.

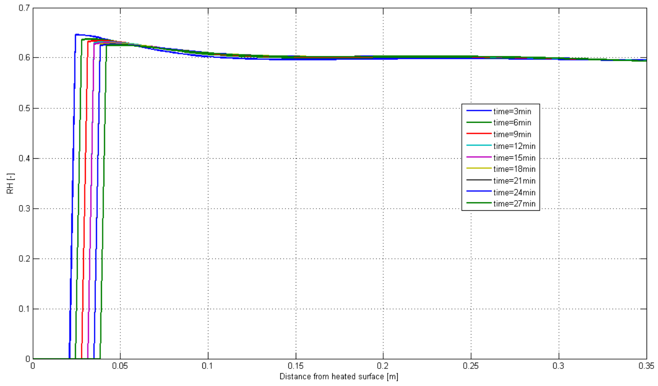

Figure 9.9. Relative humidity

The moisture clog can be seen as a sharp front/line separating the moist from dry material. Near the exposed surface the material is dry, the relative humidity is equal to 0, whereas after the front there is moist, the relative humidity is around 0.55. Also the cumulation of water that increases the relative humidity above its initial value can be seen by the jump present near the begining of the saturations front.

From the physical point of view, the transition between 0 RH and the jump should be smoother, pointing out a less suddent decrease of the relative humidity near the surface.

The accuracy of the plot depends very much on the number of elements used. Due to lack of computational power, the number of elements was limited and the results are just approximate. Even so, the trend of the relative humidity is correct and it was possible to make a right interpretation of the physical meaning.

9.2.2 Gas pressure

At the position of the moisture clog the gas pressure is increased. The gas pressure can be seen in figure 9.10. The values of the pressure increase as time passes and than they move more and more inside the concrete core. The peaks of the pressure are situated around where the temperature has approximate values of 200°C, temperature where it is assumed that all moisture has evaporated.

Like in the previous plots, the concentration of the peak pressures is very close to the exposed side, in the first 4cm from the heated surface. The value of the peaks is around 1.5MPa, that is way lower than the tensile strength of concrete (for the C50/60 that is considered as the first class of HPC, the tensile strength is 4.1MPa). This result can conclude that explosive spalling is not a consequence of the build up of pore pressures alone. The generated peaks of course will influence and increase the tensile stress and helping the promotion of cracking, but they are not the main factor.

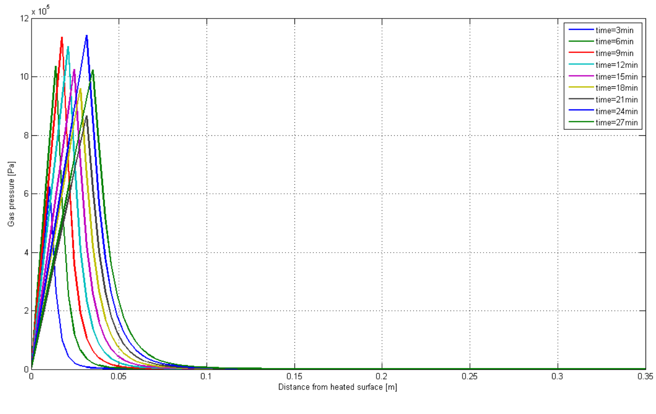

Figure 9.10. Gas pressure distribution

As seen from the exposed results, an increase of the temperature, capillary pressure and corresponding decrease of relative humidity takes place only in the vecinity of the heated surface, in the range of 0 to 5cm. Temperatures above 100°C imply evaporation of water and dehhydratation in the respective zone along with increased gas pressures. Under this conditions spalling is very possible to occur.

9.3 Stress state numerical results

The results concerning the stress state are given in terms of thermal and shrinkage strain and effective stresses. The total stress represents an approximative result of the real case.

9.3.1 Thermal and shrinkage strains

The dilatation strains are shown in figure 9.11. They are plotted according to the temperature. In the begining, when the temperature has ambient values, the thermal strain is close to 0 and then is starts increasing. The shrinkage strain starts from a value close to 0 and then increases, but in the opposite way than the thermal one. As seen from the figure, the thermal strains are higher than the shrinkage ones.

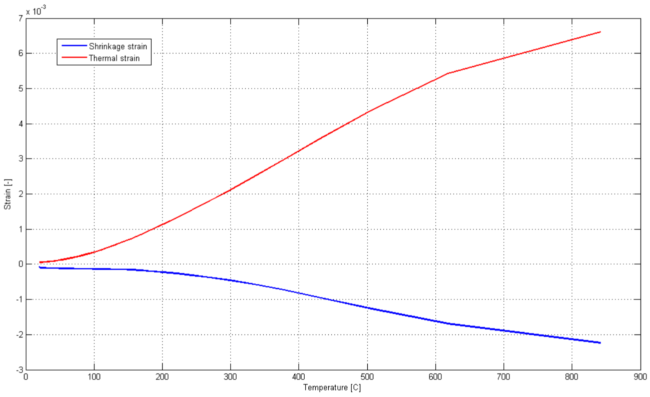

Figure 9.11. Thermal and shrinkage strains

As a validation of the results, the strains were compared with the values obtained by [Gawin et al., 2004] in their experimental and numerical work. The values are close and the trend as well, the differences that apear might be because of different values of parameters involved, such as Young's modulus, or the thermal dilatation (shrinkage) coefficient, number of elements, etc. As the parameters that need to be taken into account are some many and can vary in different ranges (for example, Young's modulus is different depending on the concrete type and also its decrease according to temperature can vary), the results are acceptable.

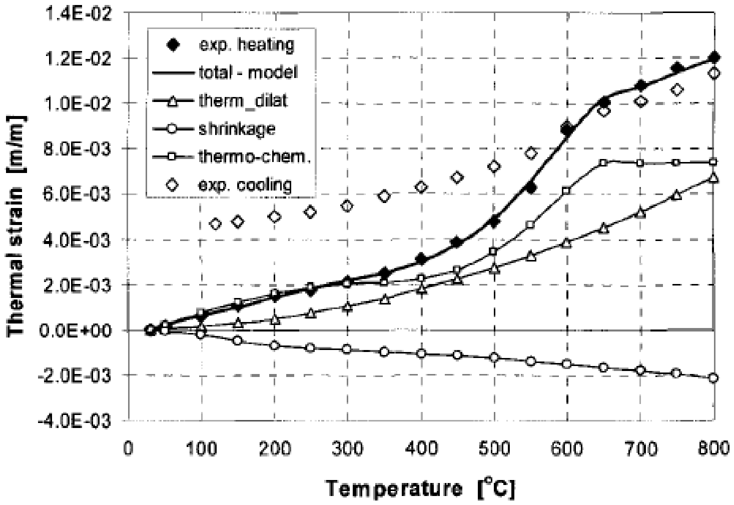

Figure 9.12. Thermal and shrinkage strains by [Gawin et al., 2004]

Even though not that relevant in this case, the final transient strains can be seen bellow. They were later on used for computing the stresses.

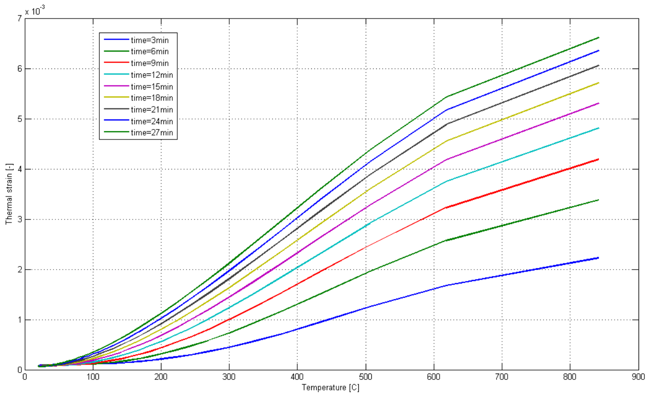

Figure 9.13. Transient thermal strains

9.3.2 Stresses

The stresses were computed from both shrinkage and thermal strains using the *Initial strain method* described before.

The effective stresses on the y direction can be seen in figure 9.14. On this direction compression stresses are developed.

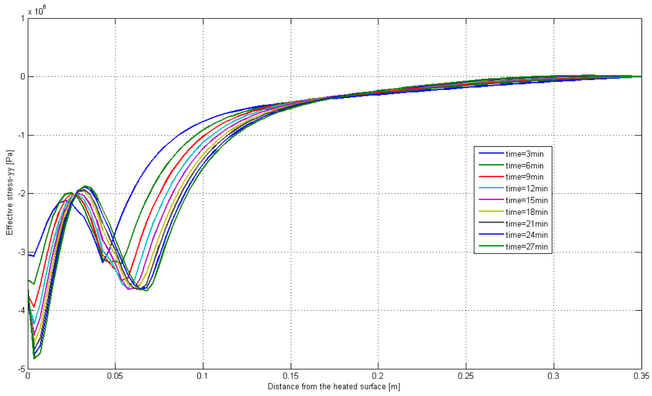

Figure 9.14. Effective stress on the ydirection

The effective stresses on the x direction can be seen in figure 9.15. At a closer look at this figure and figure 9.10 it can be noticed that the position of the maximum gas pressure does not coincide with the zone of the highest tensile stresses. This can be a strong motif that shows that the gas pressure alone cannot generate explosive spalling. The tensile stresses are high and they exceed the concrete tensile strength. This can cause serious damage, like degradation of material strength properties and cracks.

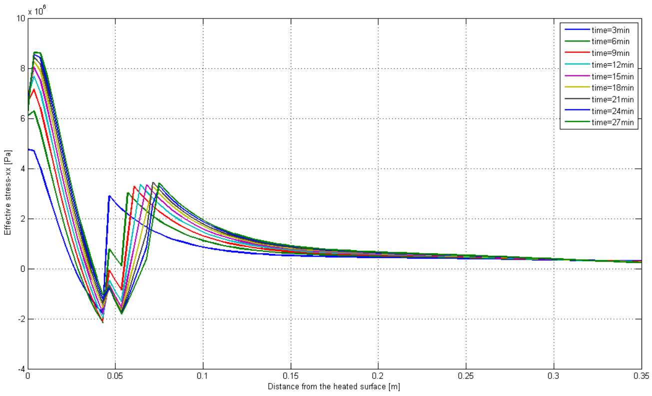

Figure 9.15. Effective stress on the x direction

An example was made when the member was loaded with an axial external force of 40MPa on the x direction. The obtained stresses can be seen below.

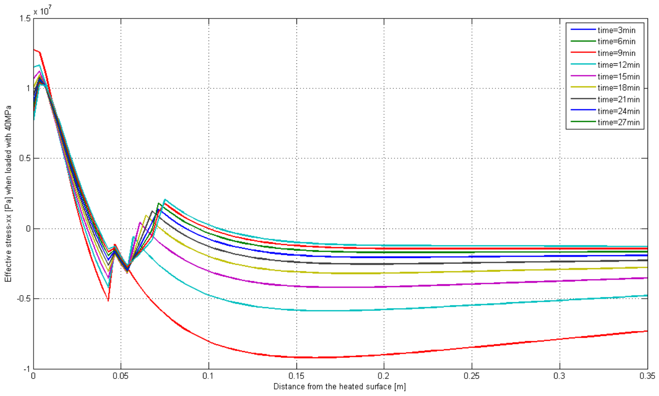

Figure 9.16. Effective stress on the x direction with a load of 40MPa

In both cases an increase of the stresses can be noticed. This external compressive load intensifies the material degradation.

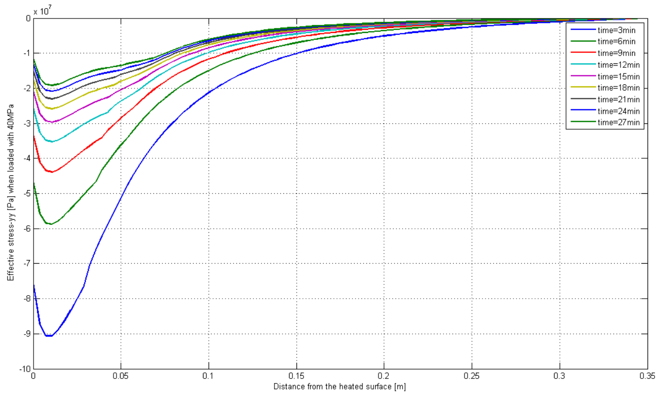

Figure 9.17. Effective stress on the y direction with a load of 40MPa

9.4 Summary

This chapter presents the temperature distribution, the capillary pressure from which the relative humidity was computed and the gas pressure. From the mechanical point of view, strains and stresses are presented. The accuracy of these results depends mainly on the input parameters. In some of the distributions the parameters were taken from experimental works and the values vary from case to case. In the case of the strains, the result does not include the thermo-chemical strain and the element is not loaded mechanically, therefore the elastic strain was composed only from shrinkage strain. These also had an influence on the stresses.

Another aspect that needs to be taken into account is the computational power. Because the present case involves a transient problem there are two aspects that need to be considered, first the number of elements used and than the time steps. The combination of these two requires a lot of computational power and storage capacity, especially for calculating the strains and stresses where also the geometry of the member was more complex.

The temperature distribution indicates a fast heating rate that influences the development of thermal stresses and rapid formation of vapors. The moisture clog indicates the position where a layer of saturated liquid forms.

The peak of the vapor pressures did not coincide with the position of the highest tensile stresses, therefore it can be confirmed that the pore pressure does not cause spalling. Also the values of the peaks did not exceed the tensile strength of the concrete. The failure will occur because of the tensile stresses that over goes the tensile strength of concrete. This effect is also enhanced by the vapor pressure.

CHAPTER 10

Conclusions

This chapter contains a sum up of all the previous chapters. An overall conclusion about the spalling phenomenon and about the used models is illustrated. A conclusion about the obtained results is carried out along with some future recommandations and improvements.

As an overall, concrete it is known to have a good behavior in fire because of its low thermal conductivity. But when it comes to types of concrete such as high performance concrete or high strength concrete several accidents were reported through time and serious damaged occurred, damage concerning human safety but also structural damage in terms of stability and integrity. Of course, all these come with severe economic consequences as well. All these factors indicated that "new" types concrete exposed to fire represents an important problem that needs further research to be carried out in order to provide a design able to prevent and predict explosive spalling of concrete.

10.1 Overall conclusions regarding the phenomenon and used models

The spalling process is a result of the heat penetrating the concrete element and as a result water will evaporate from the concrete pores. When encountering temperatures above $100°C$, the water will go through a phase change that coincides with an increase in the pore pressure, which in change will drive the water vapor flow. The water flow is driven in the direction of the exposed surface as well as in the concrete core, when meeting the proper conditions will transform back into water. In time, this condensation will develop gradually a saturated layer, called moisture clog or saturation front that will behaves as an impermeable wall for the gas flow. As a consequence the vapor pressure will build up in this region. Because of temperature propagation and water evaporation thermal stresses are developed inside the element. All these effects indicate the possibility of explosive spalling occurrence by detach of the concrete layer in front of the saturation front.

These "facts" were modeled progressively, starting from investigating parameters involved (thermal, hygral and mechanical) in concrete exposed to fire, then providing a physical model, a mathematical one and in the end a numerical one. From the begining, the physical model was divided in two sections, a thermo-hygral (or a heat-flow) model regarding heat (temperature) and mass transfer (moisture, gas) and a mechanical model concerning strains and stresses. The mathematical and numerical model were developed following this idea.

The thermo- hygral model was modeled using the following:

- Temperature
    1. Heat conduction
    2. Fourier's law
    3. Enthalpy flows due to moisture movement and phase change
    4. Unknown: temperature
- Moisture content
    1. Moisture = liquid water + water vapor
    2. Capillary conduction
    3. Surface diffusion
    4. Darcy's law, Fick's law
    5. Unknown: capillary pressure
- Gas pressure
    1. Gas = water vapor + dry air
    2. Diffusion of gas particles
    3. Darcy's law, Fick's
    4. Unknown: gas pressure

The mechanical model is supported by the next steps:

- Simplification of the total strain → consider only thermal and shrinkage strains
- Elastic stress/strain relation
- Initial strain method

10.2 Conclusion regaring the results and further development

- Because the present model is based on a pure computer simulation therefore limitations (computational power) and simplifications (chemical reactions neglected, constant values for parameters that in reality are temperature dependent, etc.) had to be adopted. An ideal case will be to combine a numerical model with an experimental one.
- The developed model used a lot of parameters that still need further research, such as degree of saturation with liquid water that further on influences the permeability and porosity. In the literature, values for permeability can differ up to a range of 10^{-4}. Also there was a lack of mathematical expression for calculating strains as thermo-chemical or transient thermal.
- Permeability is a leading factor in the whole process. An increased permeability will enhance the formation and value of the vapor pressure and a decreased permeability will act in the opposite way. Moreover, it has effects on the evaporation and dehydration rate as well.

- An aspect that can be considered in future works may be the energy necessary to develop cracks. Spalling process involves a lot of energy consumption. The gas pressure has an influence on the increase of the kinetic energy of the pieces of spalled concrete.
- The numerical mechanical model is computed using an elastic stress/strain relationship. Probably a more accurate design should involve a model that combines the elastic analysis with a plastic one containing plastic straining and also non-linear effects such as time dependent considerations like progressive cracks and creep.
- The heating rate plays in important, but also contradictory role. Assuming a fast heating rate, as was used in this case, involves two aspects: rapid development of micro-cracks that increase the permeability and in this way the pore pressure will be reduced and more vapor will flow outward. On the other hand, the water inside transforms faster into vapors making that the rate of vapor is higher than the rate of vapor escaping, resulting in a formation of an early moisture clog.
- The moisture clog is not responsible for explosive spalling. The vapor pressure that has its peak at the position of the saturation front does not reach such high values that exceed the tensile strength of the concrete, especially for HPC or HSC that have higher tensile strength. The effect of these peaks will influence the stress state and may cause local damage.
- In this thesis only the heating phase is taken into account. A more close to reality model should include also the cooling phase that has an imporant role as well from a structural perspective

Bibliography

Aïtcin and Neville, 1993. Aïtcin and Neville. *High Performance Concrete demnystified.* Magazine of Concrete Research, 1993.

Bažant and Kaplan, 1996. Zdenek P Bažant and Maurice F Kaplan. *Material Properties and Mathematical Models.* Longman Group Limited, 1996.

Bastami, Chaboki-Khiabani, Baghbadrani, and Kordi, 2011. M. Bastami, A. Chaboki-Khiabani, M. Baghbadrani, and M. Kordi. *Performance of high strength concretes at elevated temperatures.* Scientia Iranica, 2011.

Beard and Carvel, 2005. Alan Beard and Richard Carvel. *The Handbook of Tunnel Fire Safety.* Thomas Telford Publishing, 2005.

Benes and Mayer, 2007. Michael Benes and Petr Mayer. *Coupled model of hygro - thermal behavior of concrete during fire.* Journal of computational and applied mathematics, 2007.

BOŠNJAK, OŽBOLT, SHARMA, and PERIŠKIC, 2010. J. BOŠNJAK, J. OŽBOLT, A. SHARMA, and G. PERIŠKIC. *Permeability of concrete at high temperatures and modeling of explosive spalling.* VIII International Conference on Fracture Mechanics of Concrete and Concrete Structures, 2010.

Buchanan, 2001. Andrew Hamilton Buchanan. *Structural Design for Fire Safety.* John Willey, 2001.

Clausen, 2009. Johan Clausen. *Lecture of Finite Element Method.* 2009.

D.Cook, S.Malkus, E.Plesha, and J.Witt, 2002. Robert D.Cook, David S.Malkus, Michael E.Plesha, and Robert J.Witt. *Concepts and Applications of Finite Element Analysis.* John Wiley and Sons, 2002.

Heijden, 2006. G.H.A.van der Heijden. *Moisture transport and clogging of concrete under fire conditions*, 2006. URL `http://www.phys.tue.nl/nfcmr/Restop30.html`.

D.Gawin, F.Pesavento, and B.A.Schrefler, 2005. D.Gawin, F.Pesavento, and B.A.Schrefler. *Towards prediction of the thermal spalling risk through a multi-phase porous media model of concrete.* Computer methods in applied mechanics and engineering, 24, 2005.

Bèton, 2008. Fèderation-Internationale du Bèton. *Fire design of concrete structures-structural behaviour and assessment.* Bulletins, 2008.

EC2-EN1992-1-2, 2005. EC2-EN1992-1-2. *Eurocode 2: Design of concrete structures, part 1-2.* Standards Policy and Strategy Committee, 2005.

Fu and Li, 2010. Yufang Fu and Lianchong Li. *Study on mechanism of thermal spalling in concrete exposed to elevated temperatures.* Materials and Structures, 2010.

Gawin, Pesavento, and Schrefler, 2002. D. Gawin, F. Pesavento, and B.A. Schrefler. *Modelling of hygro-thermal behaviour of concrete at high temperatures with thermo-chemical and mechanical material degradation.* Compute methods in applied mechanics and engineering, 2002.

Gawin, Pesavento, and Schrefler, 2004. D. Gawin, F. Pesavento, and B. A. Schrefler. *Modelling of deformations of high strength concrete at elevated temperatures.* Materials and Structures, 2004.

Hertz, 2005. K. D. Hertz. *Concrete strength for fire safety design.* Magazine of Concrete Research, 57, 2005.

J.C.Marechal, 1972. J.C.Marechal. *Creep of concrete as a function of temperature.* International Seminar on Concrete For Nuclear Reactors, 1972.

Kaicheng, Zhonghe, and Yue, 2008. Huo Kaicheng, Shui Zhonghe, and Li Yue. *Determination of the Thermal Expansion Coefficient of Concrete at Early Ages by Using Temperature-stress Testing Machine.* Journal of Wuhan University of Technology-Mater, 2008.

Kassir, Bandyopadhyay, and Reich, 1996. *M.K. Kassir, K.K. Bandyopadhyay, and En. Reich*, 1996.

Lamont, 2006. Susan Lamont. *The Cardington and Broadgate Fires*, 2006. URL `http://911research.wtc7.net/mirrors/guardian2/fire/cardington.htm`.

Majumdar, 2005. Pradir Majumdar. *Computational methods for and mass transfer.* Taylor and Francis, 2005.

Mathew and Paul, 2011. G. Mathew and Mathews M. Paul. *Mix design methodology for laterized self compacting concrete and its behaviour at elevated temperature.* Construction and Building Materials, 2011.

Mifflin, 2006. Company Houghton Mifflin. *The free dictionary*, 2006. URL `http://www.thefreedictionary.com/relative+humidity`.

M.Zeiml, D.Leithner, Lakner, and H.A.Mang, 2005. M.Zeiml, D.Leithner, R. Lakner, and H.A.Mang. *How do polypropylene fibers improve the spalling behaviour of in-situ concrete?* Cement and Concrete Research, 36, 2005.

N.Ottosen and H.Peterson, 1992. N.Ottosen and H.Peterson. *Introduction to Finite Element Method.* Prentice Hall Europe, 1992.

P.Kalifa, F.D.Menneteau, and D.Quenard, 2000. P.Kalifa, F.D.Menneteau, and D.Quenard. *Spalling and Pore Pressure in HPC at High Temperatures.* Cement and Concrete Research, 30, 2000.

R.W.Lewis, K.Morgan, 1996. H.R.Thomas-K.N.Seetharamu R.W.Lewis, K.Morgan. *The finite element method in heat transfer analysis.* John Willey and Sons, 1996.

Heijin and Bijnen, 2007. G.H.A van der Heijin and R.M.W. van Bijnen. *Moisture transport in heated concrete, as studied by NMR and its consequence for fire spalling.* Cement and Concrete Research, 37, 2007.

Yaquba, Bailey, Nedwell, Khana, and Javeda, 2011. M. Yaquba, C.G. Bailey, P. Nedwell, Q.U.Z. Khana, and I. Javeda. *Strength and stiffness of post-heated columns repaired with ferrocement and fibre reinforced polymer jackets.* Construction and Building Materials, 2011.